Radiation Measurements 168 (2023) 106978

Contents lists available at ScienceDirect

Radiation Measurements

journal homepage: www.elsevier.com/locate/radmeas

Assessment of ambient dose equivalent rate distribution patterns in a forested-rugged terrain using field-measured and modeled dose equivalent rates

Misa Yasumiishi [a,*], Pedram Masoudi [b], Taku Nishimura [c], Kotaro Ochi [d], Xiang Ye [e,f], Jared Aldstadt [a], Mikhail Komissarov [g]

[a] Department of Geography, State University of New York, The University at Buffalo, 105 Wilkeson Quad, Ellicott Complex, Buffalo, NY, 14261, USA
[b] Geovariances, 44 Avenue des Valvins, 77210, Avon, France
[c] Laboratory of Soil Physics and Soil Hydrology, Graduate School of Agricultural and Life Sciences, The University of Tokyo, Yayoi 1-1-1, Bunkyo-ku, Tokyo, 113-8657, Japan
[d] Collaborative Laboratory for Advanced Decommissioning Science, Japan Atomic Energy Agency, 45-169 Sukakeba, Kaihama-aza, Haramachi, Minamisoma, Fukushima, 975-0036, Japan
[e] Research Institute for Smart Cities, Shenzhen University, Shenzhen, Guangdong 518060, China
[f] School of Architecture and Urban Planning, Shenzhen University, Shenzhen, Guangdong, 518060, China
[g] Ufa Institute of Biology UFRC, Russian Academy of Sciences, Pr. Oktyabrya 69, Ufa, 450054, Russia

ARTICLE INFO

Keywords:
Environmental modeling
Multivariate adaptive regression splines
Nuclear accident
Radioactivity
Topography

ABSTRACT

Measuring radioactivity in forested mountainous areas is challenging owing to the limited accessibility on foot and the canopy blocking of airborne survey signals. Meanwhile, the influence of multiple environmental factors on radioactivity, in particular on ambient dose equivalent rates (ADER) in a forested area, are not well understood. In this study, we surveyed the ADER using hand-held and backpack-type scintillators in a forest of deciduous and evergreen trees in Iitate Village, Fukushima Prefecture, Japan, on multiple dates. The village is located 35 km northwest of the Fukushima Dai-ichi Nuclear Power Plant (FDNPP). The observations showed that, 7.5 years after the FNDPP accident, the ADER still exceeded the maximum permissible level (0.23 μSv h^{-1}) of the Japanese standard limit. The ADERs were distributed unevenly in the forest, ranging from 1 μSv h^{-1} to 3.73 μSv h^{-1}, with statistically significant variabilities among survey dates. The spatial variabilities of the ADER among the survey dates were depicted by semivariograms. The effects of the complex topography on the ADER were examined using multivariate adaptive regression splines against five selected topographic parameters. Although the topographic effect of individual parameters varied between survey dates, when all topographic parameters were considered, the model predictions yielded a positive correlation ($R^2 > 0.54$). We discovered ground wetness as the source of ADER variations among survey dates based on climatic records. Additionally, we estimated the ADER from radiocesium concentrations in soil samples and checked their consistency with the measured ADER. It was found that about half of the ADER estimated from the soil samples were within the range of field measurements. Although challenges remain in the modeling of radioactivity pathways under natural conditions, this study shows that combining topographic features, meteorological factors, and near-ground and high-altitude surveys are the keys to understanding radiation behavior in the environment.

1. Introduction

In March 2011, a magnitude 9.1 earthquake struck off the Pacific coast of Tohoku, Japan, triggering a devastating tsunami that hit coastal areas. The tsunami caused the Fukushima Dai-ichi Nuclear Power Station/Plant (FDNPS/FDNPP) to suffer a meltdown and hydrogen explosions as it lost the electric power needed to cool its nuclear reactors (IAEA, 2015). Radionuclides were discharged as a consequence of the accident and they contaminated nearby regions (IAEA, 2015). Due to the meteorological conditions following the accident, the 50–70 km long

* Corresponding author.
E-mail address: misayasu@buffalo.edu (M. Yasumiishi).

https://doi.org/10.1016/j.radmeas.2023.106978
Received 19 March 2023; Received in revised form 11 June 2023; Accepted 28 June 2023
Available online 10 July 2023

and 20 km wide area northwest of the FDNPP received radionuclide fallout (Chino et al., 2011). Among the various radionuclides released from the plant, anthropogenic ^{134}Cs and ^{137}Cs in large quantities (^{134}Cs: 8.3–5.0 and ^{137}Cs: 7–20 PBq [petabecquerel = 1×10^{15} Bq]) (IAEA, 2015) were deposited dominantly in Fukushima Prefecture, while another vast portion (9–27 PBq) was released into the North Pacific Ocean (Bailly du Bois et al., 2012; Nakano and Povinec, 2012). Owing to the long half-life of ^{137}Cs ($T_{1/2}$ = 30.17 years), its negative ecological impact remains in the region, and is a significant concern.

Internal and external exposure to ionizing radiation poses risks to human health, including but not limited to the development of cancer (Cruz-Suarez et al., 2001; Tsuda et al., 2015). Even if ambient dose equivalent rates (ADER) are low, the health risks from long-term exposure to low-dose radiation are concerning (Valentin, 2005; Daniels and Schubauer-Berigan, 2011). The Japanese government established a maximum permissible level (MPL) of 1 mSv yr^{-1} as an acceptable level of airborne exposure, which is calculated at 0.23 μSv h^{-1} (0.19 μSv h^{-1} from the FDNPP accident and an average of 0.04 μSv h^{-1} background radiation in Japan). To minimize radiological health risks, environmental decontamination has been conducted in areas where the ADER exceeds 0.23 μSv h^{-1}. Generally, such operations have been successfully accomplished in contaminated urban areas (Yasutaka and Naito, 2016; Fujiwara et al., 2017). Yoshimura (2022) noted that the ADER in urban areas decreased faster than that in other land use areas with permeable surfaces owing to the extensive ^{137}Cs wash-off from pavements and sewers. In contrast, decontamination activities in forested areas are far more difficult to carry out, and ^{137}Cs will remain in a forest for a longer time (Somboon et al., 2018). Moreover, in comparison with open lands, forested areas accumulated more radionuclides and emit higher ADER (Basuki et al., 2020; Hashimoto et al., 2022).

Following the accident, numerous airborne and ground surveys were conducted to assess the distribution of ADER. Airborne gamma-ray surveys used a manned helicopter (Sanada et al., 2018), an unmanned helicopter (Sanada et al., 2019), or a drone (Sasaki et al., 2019). On the ground, gamma-ray scintillators were carried by humans or mounted on vehicles (Tanigaki et al., 2015; Andoh et al., 2019; Sato et al., 2019). Although approximately 70% of Fukushima Prefecture is forested (Ministry of Agriculture, Forestry and Fisheries, Japan, 2017), the ground survey sites were primarily in the lowlands because of the limited accessibility on foot or by vehicle in the rugged forested areas. It is worth noting that besides direct measurements of the ADER, various machine learning-based prediction methods have also been used recently (Sun et al., 2022). Malins et al. (2015a) indicated the potential influence of topography on air dose measurements using a numerical approach involving two topographic models.

The uneven topography influences where the fallout radionuclides accumulate and translocate and, thus, where they are adsorbed into the soil particles (Walling et al., 1996; Quine et al., 1997; Walling and He, 1999). Because of this adsorption mechanism, radiocesium is immobile in soils (Korobova, et al., 1998; Chibowski et al., 1999) but can migrate into the subsurface via infiltration (Ritchie and McHenry, 1990; Schimmack et al., 1994; Kato et al., 2012; Nakanishi et al., 2014). This migration also is facilitated by leaching and by the activities of soil biota (Korobova et al., 2007; Jagercikova et al., 2014). The resulting ground radionuclides concentrations affect the ADER in the area (Jacob et al., 1994; Malins et al., 2015b). Studies suggest that local topography may explain the heterogeneity of ADER in forested areas (Atarashi-Andoh et al., 2015; Imamura et al., 2020). For example, Komissarov and Ogura (2017), during an investigation in Miyagi Prefecture three years after the FDNPP accident, found that the ADER was higher in the middle and lower parts of the grasslands and forested slopes, where radiocesium concentrations in soils were higher than in the elevated areas. They explained that radionuclides migrate downward on sloped surfaces due to erosional processes (e.g., surface runoff during rainfall or snowmelt) and accumulate in the lower gradient areas. Additionally, in a forest, tree types will influence the spatial variability of fallout depositions on the forest floor and the contamination levels (Koarashi et al., 2012; Kato et al., 2018a; Kurihara et al., 2018). Kato et al. (2018a) found that the radiocesium inventory and the ADER decreased in relation to tree types in the following order: loose-flower hornbeam (*Carpinus laxiflora*) > jolcham oak (*Quercus serrata*) > redvein maple (*Acer rufinerve*).

The modeling of the ADER distribution in forested areas is particularly challenging, not only because of the poor accessibility on foot but also because of the multiple influencing factors—topography, soils, vegetation, and so on. At the same time, because nuclear power plants and other nuclear-related facilities are often built in remote mountainous areas (Hanna et al., 1982), understanding the topographic effects on environmental radioactivity is crucial when assessing radiological effects on humans and fauna in these areas. This study aimed to deepen our understanding of the topographic effects on the ADER in radiocesium-contaminated forested areas by using multi-day ADER measurements taken near the ground. By combining the ADER with ground contamination data, this study provides novel insights into the distribution patterns of environmental radioactivity in a forest and contributes to the improvement of risk assessment and decontamination measures following environmental radioactivity contamination events.

2. Materials and methods

2.1. Overview

We studied the ADER in a small basin in Fukushima Prefecture, approximately 7.5 years after the FDNPP accident, using hand-held and backpack-style scintillators on three different dates. In addition, soil samples were collected approximately at the same time and either right at the location or close to the locations of the ADER measurements. The temporal and spatial distribution patterns of the ADER were analyzed using descriptive statistics. Next, the effects of five selected topographic parameters (see Section 2.4.1) on the ADER were modeled using nonlinear regression models and semivariograms. The effects of vegetation type on the ADER were checked using ANOVA. Finally, the ADER were estimated from the vertical profiles of ^{134}Cs and ^{137}Cs contamination levels in soils, and these estimates were compared to the directly measured ADER.

In the following sections, we use the following terms to distinguish between three different types of ADER:

Actual: the ADER directly measured in the field;

Predicted: the ADER predicted by a regression model;

Estimated: the ADER estimated from the radiocesium concentration profile in soils.

2.2. Study area

The ADER were measured in Iitate Village, Fukushima Prefecture, located approximately 35 km northwest of the FDNPP (Fig. 1). At the time of sampling, part of the village was designated as a restricted zone with regulated entry, lodging, and business operations. In this village, the ^{137}Cs inventory from 300 kBq m^{-2} to more than 1800 kBq m^{-2} was deposited during the FDNPP accident (Kato et al., 2019), and the ADER at 1 m above ground were estimated 5.0–10.0 μSv h^{-1} in July 2011 (JAEA 2021), based on the results of an airborne survey conducted by JAEA in collaboration with the U.S. Department of Energy. Imanaka et al. (2012) observed a radiation exposure rate of more than 20 μSv h^{-1} in the southern part of Iitate Village during an urgent field survey (28 and 29 March 2011). Thus, data from various investigations indicated that shortly after the FDNPP accident, the ADER in the study area exceeded the MPL considerably.

The survey paths were limited to a small basin with an area of 0.56 km^2. No forest management, such as logging or pruning, had been conducted in the forest since the accident. The government had applied decontamination measures, including soil replacement in the former rice paddies and surface litter removal near trails at the bottom of the

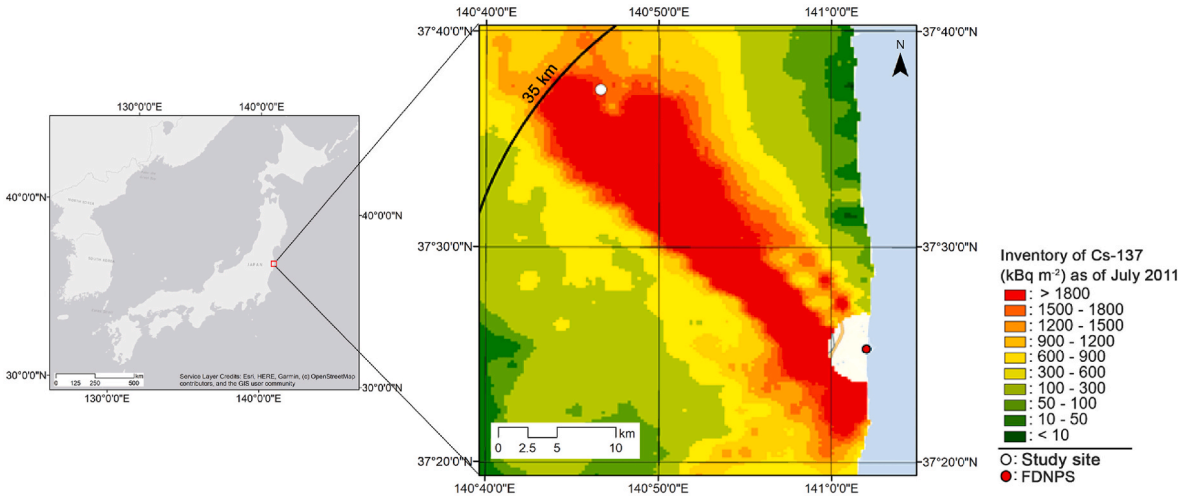

Fig. 1. Location of the study area, Iitate Village, in Fukushima Prefecture. The ^{137}Cs inventory map on the right was reconstructed based on published data (Kato et al., 2019). Maps were created using ESRI ArcMap 10.8.1.

forest. The forest comprises both deciduous and evergreen trees. The major tree types in the forest are Japanese cypress (*Chamaecyparis obtuse*) and red pine (*Pinus densiflora*), both typical dominant trees growing in central Japan (Hashimoto et al., 2022). The elevation difference from the bottom of the hill to the highest basin ridge was approximately 160 m. The slope degrees of the survey paths varied from 1° to 24°. According to the Köppen climate classification system (Beck et al., 2018), the climate of the region can be classified as a humid climate (Cfa), with an average annual precipitation of 1,362 mm and an average temperature of about 12 °C (Japan Meteorological Agency, 2019). Hillslopes exhibit microtopography with narrow creeks and varying steepness. On the ridge of the basin, at an elevation of approximately 650 m, the walking path flattens, and the landscape becomes more open. The soils of the study area, according to our data, include brown forest soils, weathered granite soil, Andosols and Inceptisol (IUSS Working Group, 2015).

2.3. ADER measurements

The ADER were measured at 1 m above ground level (AGL) on July 27, 2018, August 17, 2018, and January 12, 2019. On all survery dates, we followed a walking path that extended from the bottom of the hill to the ridge and along the ridge (Fig. 2). The path had a natural forest floors that had not been artificially cleaned or paved. Different parts of the path were covered on each survey date (Fig. 3a–c). In July and August 2018, the survey paths were shaded by the canopy, while in January, residual snow covered the ground. The ADER measurements for each survey date are presented in Section 3.1.

The hand-held NaI(TI) scintillator, Aloka TCS-172b (diameter and length: 2.5 cm; Hitachi Aloka Medical Ltd., Tokyo, Japan), was used in summer and was either hand-held or hung over the shoulders. In January, a CsI(TI) scintillator device, KURAMA-II (13.0 cm × 13.0 cm × 20.0 cm; Hamamatsu Photonics, Shizuoka, Japan), was used and was carried by the surveyor in a backpack (Tanigaki et al., 2015). Detailed specifications of both devices are listed in Supplementary Material 1. Both devices recorded additional metadata, such as date, timestamp, elevation, and latitude and longitude coordinates. The ADERs were recorded every second on July 27, 2018 and on January 12, 2019, and every 10 s on August 17, 2018. All the ADER measurements from July 27, 2018 and January 12, 2019 were then averaged into 10-s increments, which roughly corresponds to a 10-m walking distance according to a walking speed study (Azmi et al., 2012).

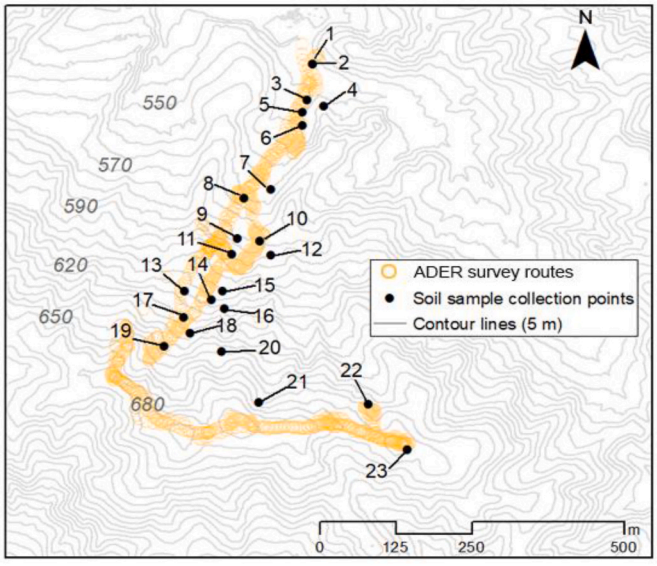

Fig. 2. Locations of ADER measurement points on all three dates and soil samples. ADER measurements by date are presented in the Results and Discussion section. Contour lines (5 m) were created using a digital elevation model (DEM) (Geospatial Information Authority of Japan).

2.3.1. Measurement comparability

This study used different models of survey devices, specifically the Hitachi Aloka TCS-172b and the KURAMA-II, to capture the ADER. Ideally, the sensitivities of multiple scintillators should be tested and compared under the same conditions. This study did not have that opportunity, which raises the question of measurement comparability. Both devices were calibrated to ^{137}Cs; however, scintillator types and their uncertainties differ (Table S1). Additionally, the two devices have structural differences. In the Aloka TCS-172b, the NaI detector is forward-looking and is placed in a photomultiplier tube (PMT) inside the handle used for carrying the device (Tanaka and Matsubara, 2012). Because of this structure, the Aloka has a strong directional dependency: the gamma-ray sensitivity toward the back of the device is weaker compared to that in the forward direction. The KURAMA-II with a CsI (Tl) scintillator uses a multi-pixel photon counter (MPPC) and captures gamma-ray and energy from all directions (Tanigaki et al., 2015). However, because the backpack-type KURAMA-II is carried on a

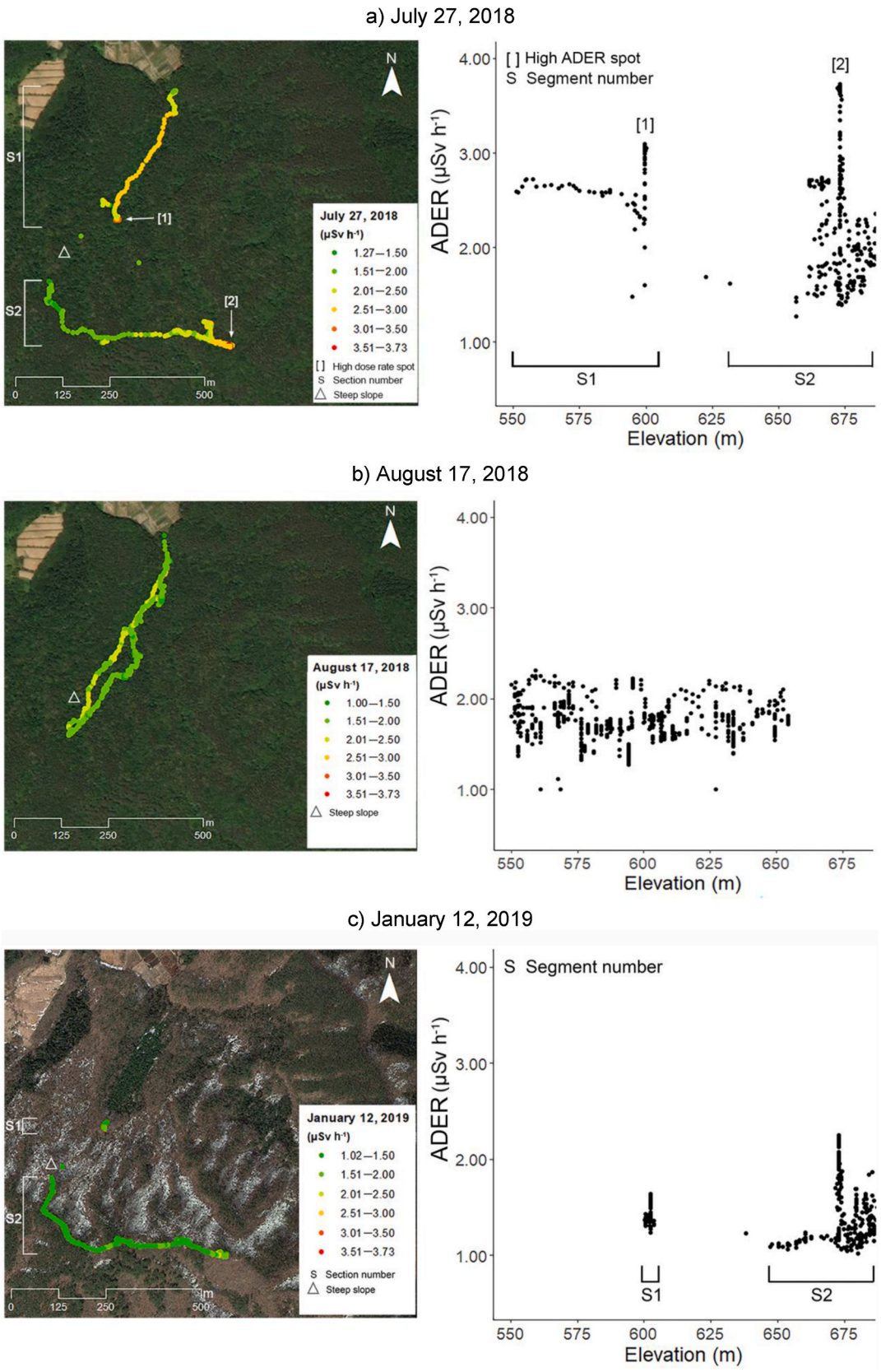

Fig. 3. (left) ADER overlaid on aerial images of the study site: a) July 27, 2018 (Image: ©ESRI 2021); b) August 17, 2018 (Image: ©ESRI 2021); c) January 12, 2019 (Image: ©Maxar Technologies, 2017). (right) Scatter plots of the ADER with elevation (m). [1] and [2] on the July map show the locations of the above 3.00 μSv h^{-1} measurements. "S1" and "S2" are added to the July and January maps and plots to show the spatial segments against elevation. White triangles indicate areas with a steep slope that were not covered by surveys on July 27, 2018 and January 12, 2019.

person's back, the human body could act as a shield affecting the energy captured by the device.

Sato et al. (2019) surveyed gamma-ray ADER in the living environment of Fukushima Prefecture using an Aloka TCS-171b and a KURAMA-II–the same models used in our study. One of their study sites was about 5 km from our study site. Then they compared the KURAMA-II measurements with those taken with the Aloka TCS-172b. For the outdoor measurements, the correlation between the Aloka TCS-172b and the KURAMA-II was $R^2 = 0.94$ (Sato et al., 2019). Although their comparison results showed a few outliers that deviated more than 2.00 μSv h^{-1}, the number of those outliers was small. Thus, we concluded that our survey results measured using the Aloka TCS-172b and the KURAMA-II were comparable. Even if a few measurement deviations between the Aloka and KURAMA-II were to occur during the surveys, the number of those outliers would not be large enough to alter the statistical results of the study.

The ADER reported in the following sections are the total ADER, consisting of both natural (cosmogenic and terrestrial) and anthropogenic dose rates. Accurate pre-accident natural background radiation data for the forest were unavailable. The absorbed dose rates in the study site region were between 0.0360 and 0.0543 μSv h^{-1} (μGy h^{-1} in the original article) based on several sources of airborne radiation monitoring data (Sanada et al., 2020). The Environmental Radioactivity Monitoring Center of Fukushima estimated that before the FDNPP accident, for Fukushima Prefecture, the average ± standard deviation, maximum, and minimum rates in 1999 were 0.0344 ± 0.0095, 0.0640, and 0.0190 μSv h^{-1} (converted from nGy h^{-1} in the original article), respectively (as cited in Furukawa and Shingaki, 2012).

2.4. Topographic effect analysis

2.4.1. Topographic parameter extractions

To extract topographic parameters for each measurement point, we used a 10-m-resolution digital elevation model (DEM) downloaded from the website of the Geospatial Information Authority of Japan (https://www.gsi.go.jp/kiban/).

For this study, we selected five topographic parameters of geomorphological importance: elevation, slope degrees, hillslope aspect, plan curvature, and upslope distance. Elevation and slope degrees indicate the gravitational force on surface water flow as well as the translocation of soil particles (Heimsath et al., 1999; Roering et al., 1999; Martin, 2000). The hillslope aspect indicates the direction in which the slope is oriented. It affects vegetation growth, surface hydrogeology, and landscape evolution (Istanbulluoglu et al., 2008; Atarashi-Andoh et al., 2015; Ii et al., 2021). Curvature–particularly profile and plan curvatures–and slope degrees are two of the most influential factors in hydrogeology and soil transport on slopes (Moore et al., 1993; Gessler et al., 1995; Heimsath et al., 1997; Tesfa et al., 2009; Momm et al., 2012). Finally, the upslope distance, which is the distance from the sampling point to the nearest highest ridge, affects the volume and velocity of the surface water flow/runoff (Stone et al., 1994; Roering et al., 1999, 2001).

The five selected topographic parameters were extracted from the 10-m DEM for each air dose measurement point using Geographic Information Systems (GIS) applications (TauDEM [Tarboton, 2005] and SAGA GIS [Conrad et al., 2015]), together with R (R Core Team, 2018).

Among the topographic parameters, the hillslope aspect needed to be converted from the circular nature of azimuth degrees to an ordinary numerical, as 360° and 0° are equivalent. One potential solution was to apply a sine transformation. The sine value was 1 in the direction of peak ADER on each survey date and −1 in the opposite direction. The directions of the peak air doses for July 27, 2018, August 17, 2018 and January 12, 2019 were approximately 70°, 50°, and 0° (north to northeast directions), respectively. The raw aspects were transformed using the following equation:

$$aspect_{transformed} = \sin\left(aspect_{raw} + \left(\frac{\pi}{2} - aspect_{peak}\right)\right) \quad (1)$$

where $aspect_{raw}$ and $aspect_{peak}$ are the observed aspect and the aspect of the peak ADER (measured in radians), and $aspect_{transformed}$ is a transformed aspect degree between −1 and 1.

2.4.2. Nonlinear regression models

The relationships between the ADER and the topographic parameters were preliminarily investigated with scatter plots. The plots suggested that the relationships were nonlinear and that the patterns varied between survey dates. Based on these plots, multivariate adaptive regression splines (MARS) (Friedman, 1991), a nonlinear regression method, was considered the ideal method for analyzing these data.

Specifically, MARS is a nonparametric piecewise algorithm that connects linear regressions to represent the nonlinearities in the interaction between variables (Friedman, 1991). This method employs an additive function to the linear combinations of these variables (Eq. (2)). Each data point for each predictor is used as a candidate cut point, and cut points known as knots are chosen according to the decrease rate in the residual sum of squares.

$$\widehat{f}(x) = \sum_{i=1}^{k} a_i B_i(x) \quad (2)$$

where k is a knot, a_i is a constant coefficient of expansion whose values are jointly adjusted to yield the best fit, B_i is the basis function, and x is an independent variable. The basis function includes a constant (intercept), a hinge function (Eq. (3)), and the product of hinge functions.

$$\max(0, x - constant) or \max(0, constant - x) \quad (3)$$

When a MARS model is fitted, knots are automatically selected in a forward stepwise manner (Hastie and Tibshirani, 1986). The sequence of models generated from this process is evaluated by generalized cross-validation (GCV), and the model with the best predictive fit is selected (Leathwick et al., 2006). Then, MARS returns the importance ranking of the variables based on the changes in GCV for each additional predictor, the degree of freedom of the best-fit model, and the knot locations and coefficients (real values). A drawback of MARS is that it returns a large number of coefficients. The "earth" package (Milborrow, 2020) of R (R Core Team, 2018) was used for the MARS calculations.

2.4.3. Semivariogram

In addition to understanding the spatial distribution patterns of the ADER in the forest, we aimed to understand the spatial distance in which the ADER are correlated by common background factors, or spatial dependency. For this purpose, semivariograms were calculated to compare the spatial structure and the variability in the distribution of the ADER across the three survey dates. A semivariogram quantifies the variability of measured values as a function of distance (Cressie, 1986; Isaaks and Srivastava, 1989; Goovaerts, 2000; Bivand et al., 2008). Because closer measurements tend to be more similar to one another than those that are farther away (Tobler, 1970), the variability of measured values is generally expected to increase as a function of distance.The semivariogram range, where semivariance flattens out after reaching sill, is the distance beyond which the measurements are no longer correlated with one another. In other words, there are spatial factors commonly affecting sample measurements up to the range distance. The semivariogram nugget effect (larger than zero value on the y-axis at x = 0) indicates variability at a distance zero (see Fig. 5 for graphical representations of the range and nugget).

The survey routes mostly followed two azimuths, northeast–southwest (30°–210° direction) and east–west (120°–300° direction). To identify spatial dependency ranges in both directions, directional semivariograms were calculated using Isatis.neo ™ software

(Geovariances, 2021), and semivariogram ranges were identified based on the behavior of the experimental variogram. When stepwise sills appear in the semivariograms, the distance corresponding to the smallest step is considered to be the spatial dependency range. During this analysis, we decided not to remove the outliers to reveal the sensitivity of the variogram to the outliers.

2.4.4. ANOVA comparing vegetation types

The hillslope was covered with evergreen trees and deciduous trees. Because the radioactive fallout occurred in early spring, the deciduous trees had few leaves to intercept the fallout. As an additional test to examine the canopy effects on the spatial distribution pattern of the ADERs, the results of the ADER measurements were divided into two groups: under evergreen and under deciduous trees. As the tree types were roughly divided by elevation on the hillslope (evergreen trees at lower elevations and deciduous trees at higher elevations on the hillslope), the ADER were divided by elevation. In a natural vegetation sequence, the evergreen (coniferous) zone should appear at higher elevations than the deciduous trees. This sequence is reversed in the study site forest because of tree-planting operations that began over a hundred years ago.

2.5. Comparison of ground contamination and ADER

2.5.1. Soil sampling

Soil samples were collected on three dates in the summer of 2018 (July 21, 22, and 27) (Fig. 2). The number of core samples was 23. A sampling tube (5-cm diameter; 30-cm length; Daiki Rika Kogyo Co., Ltd., Saitama, Japan) was pushed into the ground using a hammer. The tube was made of metal and contained a replaceable plastic liner. Once the tube was inserted fully into the ground, the plastic liner containing the soil was pulled out, sealed, marked, and delivered to the laboratory at the University of Tokyo. The collected samples were divided into 2.0-cm depth intervals (from the surface to 20.0 cm in depth) and 2.5-cm depth intervals (20.0–30.0 cm in depth). The litter (organic layer) on the soil surface was gently removed. The collected samples mostly contained the A soil horizon (the topmost mineral layer mixed with humified or partially humified organic matter). Some samples displayed the AB horizon (the transition to the mineral layer). Among the 23 samples, seven of them have a collected depth of less than 30 cm because an object, such as a tree root, hindered the tube from penetrating into the ground or because the brittle or wet bottom soils dropped out from the tube. Those issues were noted, but repeat samples were not collected to reflect the soil characteristic at the planned sampling locations.

Soil samples were oven-dried to constant weights for approximately 24–48 h (precise drying time lengths varied depending on the soil sample dryness) at 105 °C. Soil from each dried sample was placed in a clean mortar and ground into fine pieces. The collected soils contained >50% sand on average. According to the USDA soil texture classification, most of the samples were in the categories of sand, loamy sand, sandy loam, and loam. The processed samples were stored in polyethylene vials and sent to the Isotope Facility for Agricultural Education and Research at the Graduate School of the University of Tokyo, for isotope analysis. Radioactivity levels were measured with an NaI(Tl) scintillation automatic gamma counter (2480 WIZARD2 gamma counter, PerkinElmer Inc., Waltham, Massachusetts, USA). This counter is equipped with a well-type NaI(Tl) crystal of 75 mm in diameter by 75 mm in length, covered with a lead shield of 75 mm in thickness. The energy calibration was performed using the 662 keV of gamma-rays from ^{137}Cs. The radiocesium (^{134}Cs and ^{137}Cs) concentration was calculated from the count rates in six energy windows (300–398, 524–657, 599–666, 608–706, 724–862, and 1330–1510 keV) during a 20 min measurement time. The detection limit was approximately 0.5 Bq (Osawa et al., 2018). The specific activity of ^{134}Cs and ^{137}Cs was measured in Bq kg^{-1} (by unit mass). In addition, concentration by unit area (radiocesium inventory, Bq m^{-2}) was calculated based on dry bulk density (mass of oven-dried soil/total soil volume) and soil mass. Radiocesium concentrations were not normalized to the FDNPS accident date.

2.5.2. Ground-to-air conversion

Based on the ^{134}Cs and ^{137}Cs concentrations in the soil samples, the ADER above the sample locations were estimated so that these could be compared with the actual ADER measurements. The vertical concentration parameter, or the relaxation mass depth (β: g cm^{-2}), was calculated using wet soil weight (ICRU, 1994; Ochi et al., 2022). A relaxation mass depth represents the degree of penetration of radiocesium into the soil mass. The exponential function used for evaluating β is given in Eq. (4):

$$A_m(\zeta) = A_{m,0} \exp\left(-\frac{\zeta}{\beta}\right), \quad (4)$$

where $A_m(\zeta)$ is the activity concentration of ^{137}Cs at a certain mass depth ζ (Bq kg^{-1}); $A_{m,0}$ is the activity concentration of ^{137}Cs at ground level (Bq kg^{-1}); ζ is the mass depth (g cm^{-2}), and β is the relaxation mass depth (g cm^{-2}).

Then the ADER (μSv h^{-1}) at 1 m AGL were calculated using the conversion coefficient (Eq. (5)) as described in previous reports (Saito and Petoussi-Henss, 2014; Ochi et al., 2022).

$$ADER_{CsE} = \left({}^{134}Cs_{inv} \times {}^{134}Cf\right) + \left({}^{137}Cs_{inv} \times {}^{137}Cf\right) \quad (5)$$

where ADR_{CsE} (μSv h^{-1}) is the final estimated ADER from soil Cs concentrations at 1 m AGL; and $^{134}Cs_{inv}$ and $^{137}Cs_{inv}$ are the ^{134}Cs and ^{137}Cs inventories (Bq m^{-2}) in the entire sample (30 cm depth), respectively. The ratio of ^{134}Cs to ^{137}Cs was calculated according to their decay rates, considering March 15, 2011, as day zero when the ^{134}Cs to ^{137}Cs ratio was 1:1 (IAEA, 2015). ^{134}Cf and ^{137}Cf are the ground-to-air conversion factors for ^{134}Cs and ^{137}Cs (Bq m^{-2}) based on β, respectively.

2.5.3. Estimated and actual ADER comparison

There is a hypothesis that the ADER measured in natural/field conditions and the ADER estimated from contaminated soil samples cannot be compared pairwisely, even if both are from the same place. For example, Malins et al. (2015b) demonstrated how the device height above the ground and β affected the percentages of ground-sourced gamma-radiation contributed to the ADER. They conducted Monte Carlo radiation transport calculations and showed that when a measurement device was 1 m above the ground, 60%–80% of the measured dose equivalent rate originated from 10 m around the measurement point, depending on β values, and on a plane surface with no shielding objects. This percentage increased as the radial distance from the device increased, although the increase curves differed among the isotopes. Additionally, terrain and other obstructions can block gamma-rays coming from the ground, and the angular distribution of photons against the detector surface can affect the flux of captured radioactivity (Ji et al., 2016). Paying careful attention to the complexity of this ground-to-air relationship, we descriptively examined whether the radiocesium concentrations in soils reflected local topography and whether the ADER estimated from soil samples agreed with the ranges of the surrounding ambient ADER.

3. Results and discussion

3.1. Spatial and temporal distribution patterns of ADER

The ADER were visualized by survey date and plotted with elevation (m) to show the ADER changes over the hillslopes (Fig. 3). We used different satellite images of the site for July/August 2018 and January 2019 to show the vegetation and ground condition differences between the seasons (note: the images were not of the exact survey dates). "S1" and "S2" were added to the July and January maps and plots to show the

spatial segments against elevation. White triangles indicate areas with a steep slope.

Depending on the survey routes and measurement timing, the ADER fluctuated (Fig. 3), and the highest ADER in the forest varied among the survey dates. The highest ADER, measured on July 27, was 3.73 μSv h^{-1} (Fig. 3a). Fig. 3a [1] and [2] indicate locations where the ADER were above 3.00 μSv h^{-1}. The August 17 measurements did not observe values above 3.00 μSv h^{-1} with the highest measurement being 2.31 μSv h^{-1}. On January 12 (Fig. 3c), the survey started in the middle of the ascending slope. The highest rate on January 12 was 2.25 μSv h^{-1}, near the easternmost point along the ridge, which was the same area where the July 27 measurements recorded the highest ADER (Fig. 3a [2]). The July 27 and January 12 routes overlapped in the ridge area, and the January 12 measurements displayed clear air dose reductions relative to the July measurements over the same route (Fig. 3a and c).

Fig. 4 shows the ADER distributions (median, mean, and standard deviation) on the three survey dates. The variations in the actual ADER measured on different survey dates were larger than changes caused by nuclear decay alone. For example, the smallest median difference in the measured ADER was between August 17, 2018 (1.72 μSv h^{-1}) and January 12, 2019 (1.34 μSv h^{-1}) (Fig. 4), with a decrease of 22.09%. However, the reduction by only ^{137}Cs decay between August 17, 2018 and January 12, 2019 should have been 0.93%. The significance of variations among the ADER on the three survey dates was checked with ANOVA. The ANOVA results indicated significant variance differences between the measurements for July 28 and August 17, August 17 and January 12, and July 28 and January 12 ($p < 0.001$ for all three ANOVAs). We concluded that the ADER differences among the three survey dates were statistically significant and that environmental factors, in addition to nuclear decay, affected the differences. Moreover, some of the ADER exceeded the maximum permissible level (0.23 μSv h^{-1}) of the Japanese standard limits as they ranged from 1 μSv h^{-1} to 3.73 μSv h^{-1}.

3.2. Spatial dependency ranges

Semivariograms were created for each survey date to check the spatial dependency ranges of the ADER (Fig. 5a–c). The July 27 semivariogram (Fig. 5a) showed unusual trends in that these semivariograms decreased once and then increased with lag distance. We interpreted this as a manifestation of the first sill reached within a very short distance. The semivariogram ranges on the ascending slopes were approximately <10 m on July 27 and approximately <50 m on August 17 (Figs. 5a and 5b). The semivariogram ranges at the ridge area were approximately <10 m on July 27 and < 100 m on January 12 (Figs. 5a and 5c). These results showed that the distance within which the ADER were correlated varied depending on the survey timing and path selection. Another

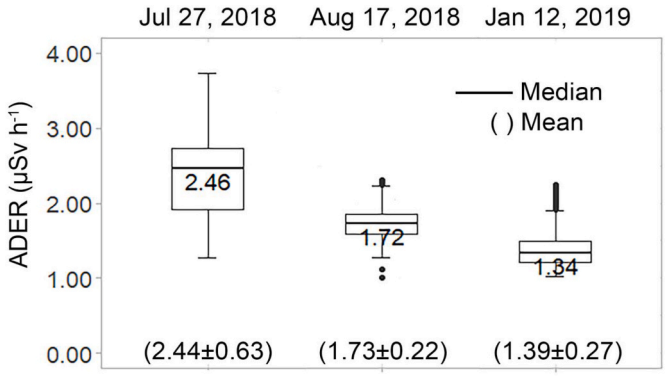

Fig. 4. Comparisons of ADER distributions and medians (μSv h^{-1}) on the three survey dates. Whiskers extend to the 1st quartile–1.5 inter-quantile range (IQR) and the 3rd quartile + 1.5 IQR.

difference between July 27 and the other two dates was that its semivariogram (γ) was one order of magnitude smaller than on August 17 and January 12. On July 27, the spatial dependency of the ADER was confined to a very short distance compared with those on August 17 and January 12. These variations in ADER and their spatial dependency ranges raised questions about why those values were not consistent in the same undulating topography on different dates and what the differences in the background factors might be. These questions led us to investigate meteorological factors.

3.3. Meteorological factors

Although the summer measurement dates were only three weeks apart, and the vegetation conditions were similar, the August ADER were closer to those measured in January than to those measured in July. Moreover, spatial dependency distances differed between July 27 and August 17. Because topography was a consistent background factor, a potential factor in these differences was the climate. We, therefore, examined the meteorological records for Iitate Village, Fukushima Prefecture (Table 1). The climatic data presented in Table 1 were recorded at a monitoring station of the Japan Meteorological Agency, which is about 6 km from the study site forest. The study area had not received significant rain for 15 days prior to the July 27 survey date (Fig. S1). However, the site received, in total, about 160 mm of rain between August 6 and 12, with 30 mm on August 16, 2018, the day before the August survey date. The soil samples were all collected in July, when the ground had not received measurable precipitation for days prior to the collections. The average water content percentages (calculated as [(wet soil weight – dry soil weight)/dry soil weight]) in the soil samples collected in July at a 10-cm depth varied from 40.8% to 100% (roughly field capacity to saturation). In August, the soil water content was expected to be higher due to precipitation in the week and on the day before the August ADER survey. On January 12, 2019, approximately 1–3 cm deep of snow was on the ground.

Gamma-ray spectrometry is used to measure soil moisture content (Baldoncini et al., 2018, 2019) based on past findings that soil moisture is inversely related to the gamma radiation signal (Carroll, 1981). Thus, soil wetness influences the ADER near the ground surface (Yoshioka, 1994) and can lead to erroneous gamma-ray readings (Erdi-Krausz et al., 2003; Mikailova et al., 2021). Schimmack et al. (1998) found that when rainfall saturated the soil, the absorbed dose rates (nGy h^{-1}) decreased by approximately 60% compared to those in dry soil. Nakanishi et al. (2022) reported that in forested areas in Fukushima Prefecture, the ADER decreased during rainfall as the soil moisture content increased. Snow cover can also cause an additional decrease in the ADER because it shields the gamma rays from the ground surface (Ishizaki et al., 2016; Omori et al., 2016). According to Nagaoka et al. (1988), the gamma-ray exposure rates (μR h^{-1}) at snow-covered sites were 17%–36% lower than the rates over bare ground. In particular, Komissarov and Ogura (2020) found that during periods of stable snow cover in Miyagi Prefecture, the ADER increased with decreasing snow thickness. This was because the measurement distance between the soil surface and the gamma survey scintillator varied due to changes in snow depth and because snow absorbed radioactive emissions and acted as a protective screen. Thus, we conclude that the soil moisture on August 17 and the snow cover on January 12 affected the ADER measurements above the ground.

Another climatic factor that varied among the survey dates was wind speed (Table 1). On August 17, 2018, the wind speed was more than twice that on July 27. The wind speed was about the same on July 27 and January 12, 2019. Based on airflow models in a forest (Yamada, 1982; Melese Endalew et al., 2006, 2009), the higher wind speeds and the openness, due to less canopy, in the ridge area on January 12 influenced airflows in the forest. However, the wind does not affect the gamma-rays emitted from masses such as soils. The strong winds move surface soil particles and change the distribution of those particles;

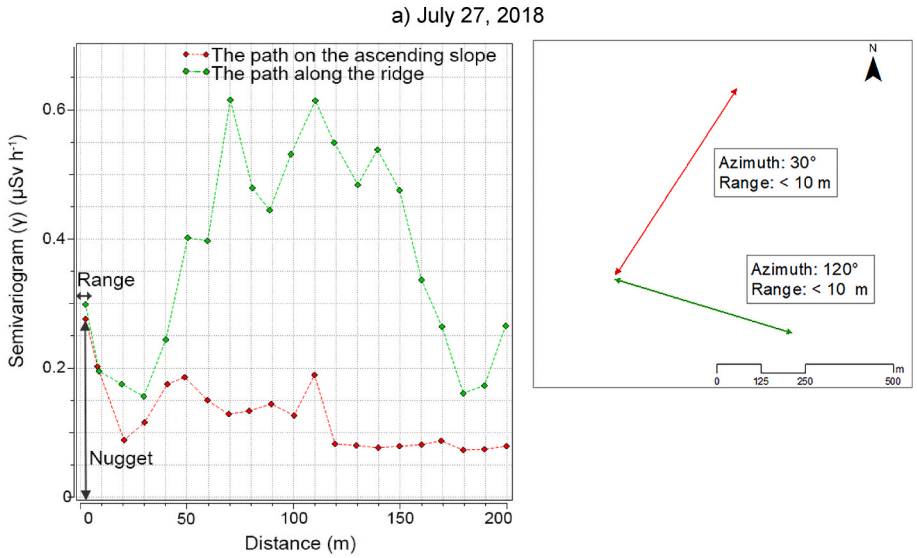

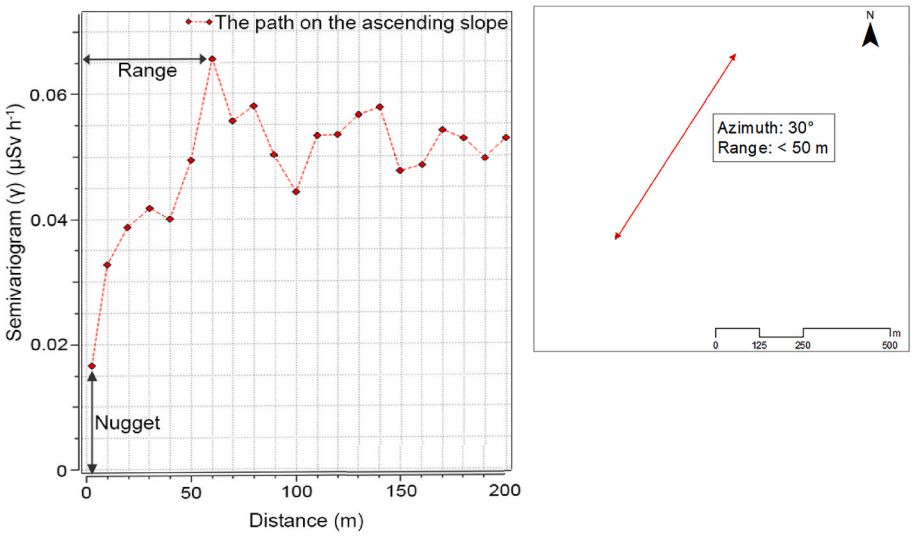

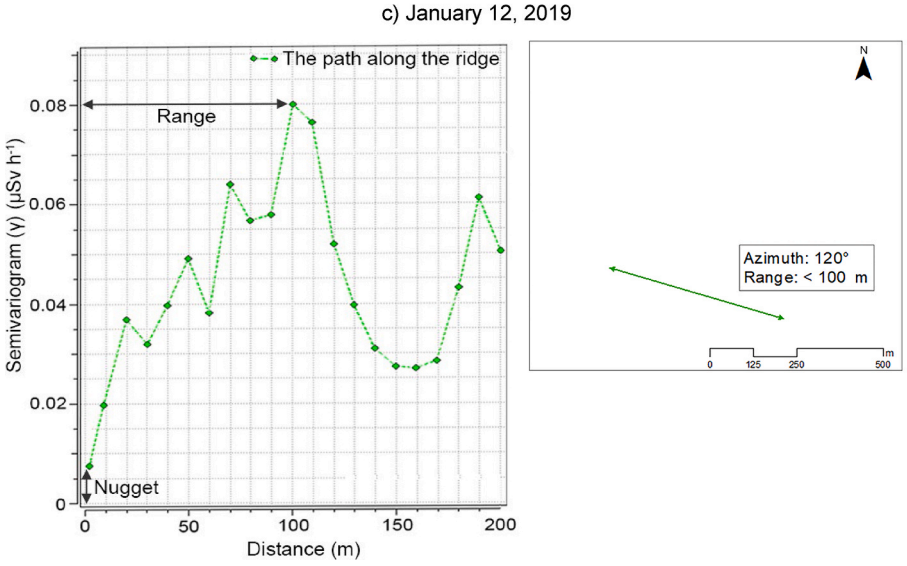

Fig. 5. Directional semivariograms on the three survey dates. (left) Semivariograms (γ) in μSv h^{-1} by walking path direction. (right) The azimuths of the survey path directions and spatial dependency ranges. In all diagrams, red represents the path on the ascending slope. Green represents the path along the ridge. Semivariogram model settings: Lag distance (a minimum separation distance between samples) 10 m; maximum model distance 200 m (calculated by Isatis. neo™ geostatistical software).

Table 1
Meteorological conditions on each survey date. The data were extracted from the Japan Meteorological Agency website (https://www.data.jma.go.jp/). Daily precipitation, hourly wind, and air temperature data are listed in Supplementary Material 2.

	July 27, 2018 (14:00–17:00)	August 17, 2018 (12:00–14:00)	January 12, 2019 (12:00–14:00)
Average air temperature (°C)	21.8	19.6	1.9
Wind direction (azimuth, °)	68–135	293–315	293–315
Average wind speed (m s^{-1})	2.9	7.6	2.9
Precipitation (mm)	0	0	0 (snow on the ground)
Number of days since precipitation and its amount (mm day^{-1})	14 days (1.0)	1 day (30.0)	13 days (1.0)

however, the effects of the suspension and redeposition of soil particles are small in a forest where the ground is well-covered by the vegetation and canopy. Thus, this study does not consider that wind speed differences were a factor of the ADER measurement variations across survey dates. However, in future studies, it would be worth examining the effect of wind on the ADER in locations where wind significantly affects surface soil suspension and wind erosions.

Considering the moisture factor, we conclude that the July 27, 2018 measurements provided the most accurate ADER readings, as they were measured above dry soils.

3.4. Topographic effects

3.4.1. Model predictions by single topographic parameters

The MARS models with a single topographic parameter demonstrated a nonlinear relationship between the ADER and the topographic parameters, and the model functions differed depending on the survey date and routes (Fig. 6). In general, the MARS models predicted that the ADER were positively correlated with elevation on July 27 (Fig. 6a E) and August 17 (Fig. 6b E), although the upward trend changed at the highest elevations. On January 12 (Fig. 6c E), the model represented an inverse trend against the elevation. The survey route on that day was confined to the ridge area with little topographic variation, and one location with an elevated ADER toward the eastern edge of the path influenced the prediction.

The models utilizing slope degrees (Fig. 6-S) displayed a consistent trend across the survey dates: the steeper the slope, the lower the ADER. This is consistent with the hypothesis suggested by Komissarov and Ogura (2020) that on steep slopes, where erosion occurs more intensively, the radiocesium is washed out faster from the soil via surface runoff, thus reducing the radionuclide concentration in the soil and, consequently the ADER. The models showed coefficient changes at approximately 5 to 11 slope degrees on all dates. However, the surveys skipped the steeply sloped area on July 27, 2018 and January 12, 2019 (area marked with triangles in Fig. 3a–c). It is possible that if the surveys had continued over that area, the model functions would have shifted according to the higher slope degrees.

In models for hillslope aspects (Fig. 6-A), the ADER showed an increasing trend toward the peak measurement directions (sine = 1.0), facing north−northeast. According to Komissarov and Ogura (2020), after the FDNPP accident, radionuclides were mostly deposited from the radioactive aerosol cloud onto land covered by snow in the Tohoku region. During the snowmelt period (April–May), the highest volumes/intensities of surface runoff were recorded on slopes with a southern aspect, medium volumes were recorded on western and eastern aspect slopes, and the lowest volumes were recorded on slopes with a northern aspect (runoff coefficients: 0.71, 0.49, and 0.38, respectively). Thus, in 2011 and in the following years, the radionuclides were washed out faster with runoff from slopes of southern, western, and eastern aspects. Whereas the lateral migration of radionuclides throughout the slope with the northern aspect was slow, leading to increased ADER due to the accumulated radionuclides in the ground. Our model results are in accordance with the fact that the survey routes were mostly on north- and northeast-facing slopes. The July 27 model for the hillslope aspects overestimated the ADER and returned an unrealistic upward trend (Fig. 6a–A [1]), owing to a greater than 1 μSv h^{-1} increase in specific aspect degrees on that day (Fig. 3a).

The MARS models predicted that the ADER would negatively correlate with the plan curvature (Fig. 6-P): the more convex the curvature (positive curvature index numbers), the lower the ADER. The upslope distance length did not have a consistent influence on the ADER. On July 27, the model for upslope distance overestimated the ADER at the point of longer upslope distance (Fig. 6a-U [2]). This overestimation suggests that, on that day, higher ADER were concentrated in an area surrounded by longer hillslopes.

The importance rankings for the individual topographic parameters in the ADER prediction varied among the survey dates as well as between routes. The hillslope aspect was consistently shown to be important, reflecting the survey path selection. Elevation was not ranked as the most important factor on any survey date but was consistently ranked at mid-level importance and never fell to #5 (least important). When the survey covered the longest range of the hillslope on July 27, upslope distance, elevation, and slope degrees were the most important factors, while plan curvature was the least important. This result indicates that when a wider area was covered, the effect of local ground curvature was obscured by the effects of larger-scale topographic structures.

The MARS model hinges and coefficients are listed in Supplementary Material 3.

3.4.2. Model predictions using all topographic parameters

The ADER were predicted by using all five topographic parameters with MARS for each survey date, and the model accuracy was evaluated using a coefficient of determination (R^2), which was at least 0.54 or larger (Fig. 7). These results show that all five topographic factors interactively influenced gamma-ray readings. Moreover, these results demonstrate the ability of MARS to overcome missing values and nonlinear relationships between the independent and dependent variables.

The July 27 (Fig. 7a) prediction result showed a row of dots at the same predicted values, indicating the limitation of the model. Examining the original data plot on that day (Fig. 3a [S2]), a wide range of ADER were measured in the ridge area around an elevation of 675 m. This model outcome indicates that other factors in the ridge area, which were not captured in the model settings, contributed to the large variations in the ADER at that elevation.

A previous study at the same site examined the relationship between topography and soil radiocesium contamination levels and found that topographic factors explained up to 46.75% of the contamination deviance (Yasumiishi et al., 2021). Combining this result with the current research, the topography could explain approximately 50% of the environmental radioactivity (50% maximum for the soils and 50% or above for the ADER) at this study site.

3.4.3. Vegetation cover impact

The July 27 and August 17 surveys were conducted in areas with deciduous and evergreen trees. Broad-leaved deciduous forests (49.1% of the forested area) and evergreen coniferous forests (47.0%) are the dominant forest types in the Fukushima Prefecture heavily affected by the FDNPP accident in Japan (Hashimoto et al., 2012). The tree canopy of the evergreen coniferous forests acted as an efficient filter for the atmospheric plume of ^{137}Cs from the FDNPP accident; therefore, a large proportion of ^{137}Cs was initially intercepted and retained by the tree

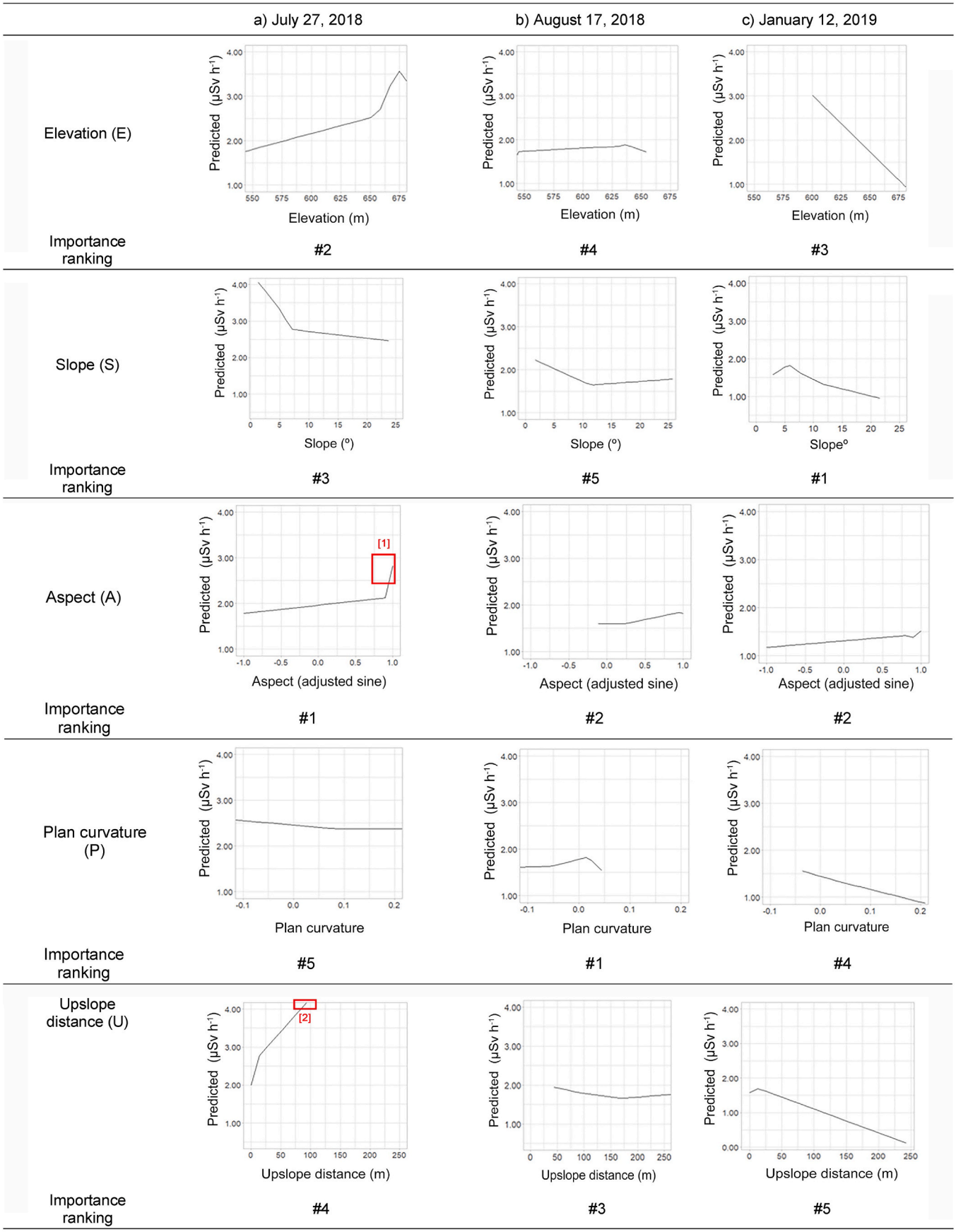

Fig. 6. MARS model predictions on each survey date for each topographic parameter. The number under each plot indicates the importance ranking of the topographic parameter. [1] and [2] indicate model overestimations.

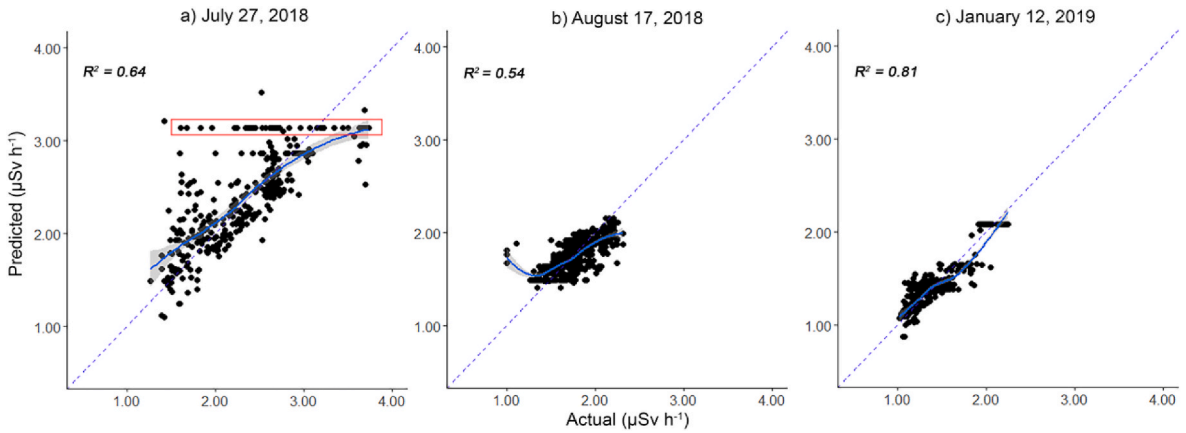

Fig. 7. Scatter plots of predicted and actual ADER on each survey date, with model equations and R^2. The solid blue lines indicate trendlines with 95% confidence intervals. The dotted blue lines indicate y = x (a perfect prediction). In the July 27 plot, a row of the same predicted values appeared, indicating a model limitation.

canopy and was subsequently transferred to the forest floor via processes such as throughfall, stemflow, and litterfall. In contrast, the canopy-interception effect was less significant in the broad-leaved deciduous forests compared to the evergreen coniferous forests because the deciduous forests were leafless at the time of the accident (Koarashi et al., 2016). Koarashi et al. (2016) found that the gamma-ray dose rates were significantly ($p < 0.01$ via the unpaired *t*-test) higher at the evergreen coniferous (Japanese cedar-dominated) forest site (0.34 ± 0.04 μSv h^{-1}) than at the broad-leaved deciduous forest site (0.26 ± 0.09 μSv h^{-1}) in the southwestern part of Fukushima City. Contrary, Kato et al. (2018b) observed that ambient dose rates in mixed broad-leaved forest and deciduous forests were higher than in evergreen conifer forests within Fukushima Prefecture.

According to the aerial winter image (Fig. 3c), the dividing point between those two tree types was at an elevation of approximately 580 m. We grouped the air dose measurements into evergreen and deciduous areas to evaluate the effects of vegetation type on ADER (Fig. 8). The areas under the evergreen trees showed higher average ADER (about 4%) than the areas under the deciduous trees in absolute measurements. However, the differences were not statistically significant. The p-values calculated via ANOVA for the mean differences between the evergreen and deciduous areas were 0.90 on July 27 and 0.30 on August 17. Thus, vegetation cover type was determined to be a non-significant factor on this hillslope.

3.5. Radiocesium distribution and comparison of actual versus estimated ADER

Total radiocesium concentrations ($^{134}Cs + {}^{137}Cs$ down to 30 cm depth) in soils were calculated and mapped (Fig. 9). The concentrations were higher at the hill bottom and in the midslope at zones of sediment accumulation with low slope gradients. Soil samples #11 (midslope) and #23 (ridge) are closest to the locations where the highest ADER were recorded (Fig. 3a [1] and [2]). The total radiocesium activity in sample #11 was the fourth-highest (434 kBq kg^{-1}), but the radiocesium activity in #23 was only the fifteenth-highest (165 kBq kg^{-1}). The spatial distribution patterns of soil contamination levels (Fig. 9) and actual ADER levels (Fig. 3) did not coincide completely. The variability of radionuclides concentrations in the soil samples confirmed the findings of past research, such as that by Kato et al. (2017), showing that radionuclide contamination in soils can be heterogeneous, even at short separation distances, and that sometimes contamination patterns are not consistent with location elevation changes.

Fig. 10 shows the vertical profiles for ^{137}Cs concentrations, relaxation mass depth (β), and ^{134}Cs and ^{137}Cs inventories for all soil samples. In all soil cross-sections (except three: #1, #2, #9), the strongest ^{137}Cs activities were found in the topmost layer. This is consistent with other investigations conducted in different parts of Japan. For example, Kato et al. (2012), Teramage et al. (2014), Konoplev et al. (2016), and Yoschenko et al. (2022) found that most (80–90%) of the fallout

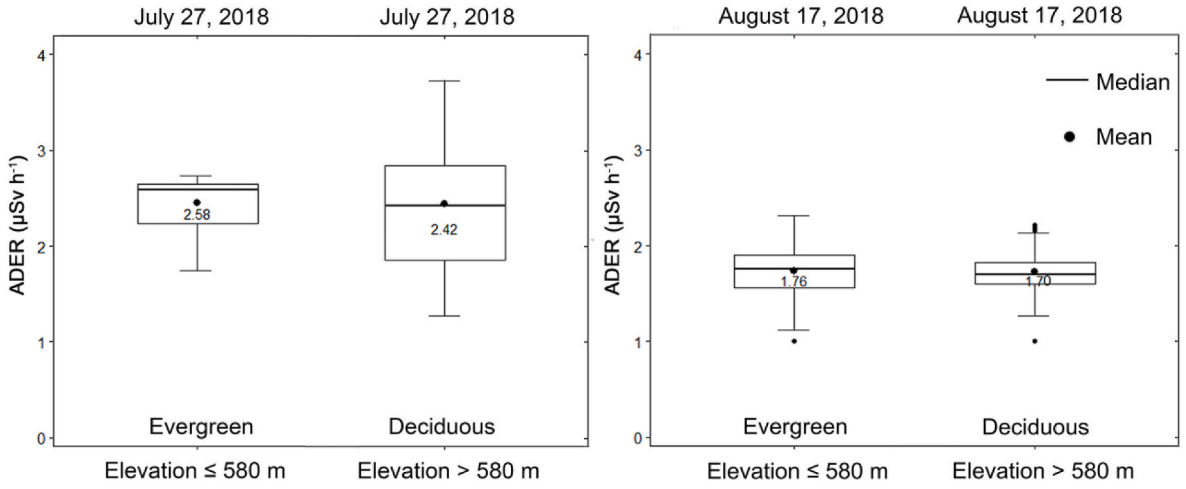

Fig. 8. ADER on July 27 and August 17 divided according to elevation: 580 m or below for the evergreen area and above 580 m for the deciduous area (horizontal solid bars: median; numbers: median values; circles: mean). Whiskers extend to the 1st quartile–1.5 inter quantile range (IQR) and the 3rd quartile + 1.5 IQR.

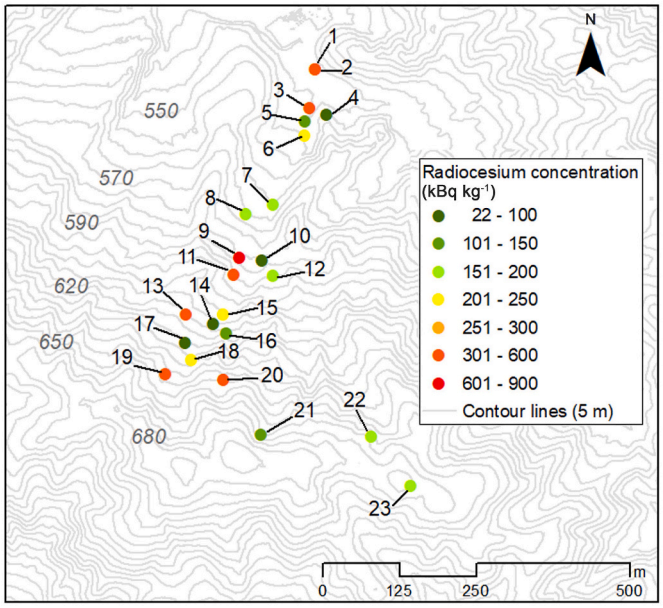

Fig. 9. Twenty-three soil sample locations with sample numbers and total radiocesium concentrations ($^{134}Cs + {}^{137}Cs$) down to a 30-cm depth (kBq kg^{-1}). Locations #1 and #2 were close, so the dots overlap. Concentrations were ranked based on geometric classification into seven levels using ArcGIS 10.8.1.

radiocesium originating from the FDNPP accident either over time, or on different observed times was found in the upper 5 cm topsoil layer. There were two reasons for the radiocesium activity peaks not being in the top soils in the three (#1, #2, #9) samples: sediment accumulation with soil particles that have eroded and translocated from upslopes, and accelerated infiltration due to water pooling on the ground surface. Particularly at sampling location #1, coarse sandy soil particles presented on the surface and displayed very low radiocesium concentrations in the top 10 cm depth. ^{137}Cs are known to be strongly adsorbed by clay mineral fractions (He and Walling, 1996; Koarashi et al., 2012; Maekawa et al., 2015). At this location, 1) fine particles had been washed away or buried by larger soil particles with lower concentrations of radiocesium, and 2) water pooling and infiltration due to a low slope gradient, had combined to result in a bell curve in ^{137}Cs accumulations with depth.

Next, the ADER estimated from the soil samples were compared with the actual readings against elevation (Fig. 11). The soil sample numbers in Fig. 11 correspond to the numbers in Figs. 9 and 10. Soil samples located less than 10 m from the ADER survey routes are marked with square boxes. About half of the ADER estimated from the soil samples were within the range of the field measurements. However, there were large variabilities among the estimated ADER, and they did not exhibit conspicuous spatial patterns with varying elevation or correlate to the actual ADER.

The estimated ADER from soil sample #9 was beyond reasonable ranges, even considering the possible heterogeneity of radionuclides contaminations in the soils. In sample #9, the maximum radiocesium concentration was not in the topmost layers, and ^{137}Cs activities exceeded a total of 500 kBq kg^{-1} at 4–8 cm depth. The estimated ADER

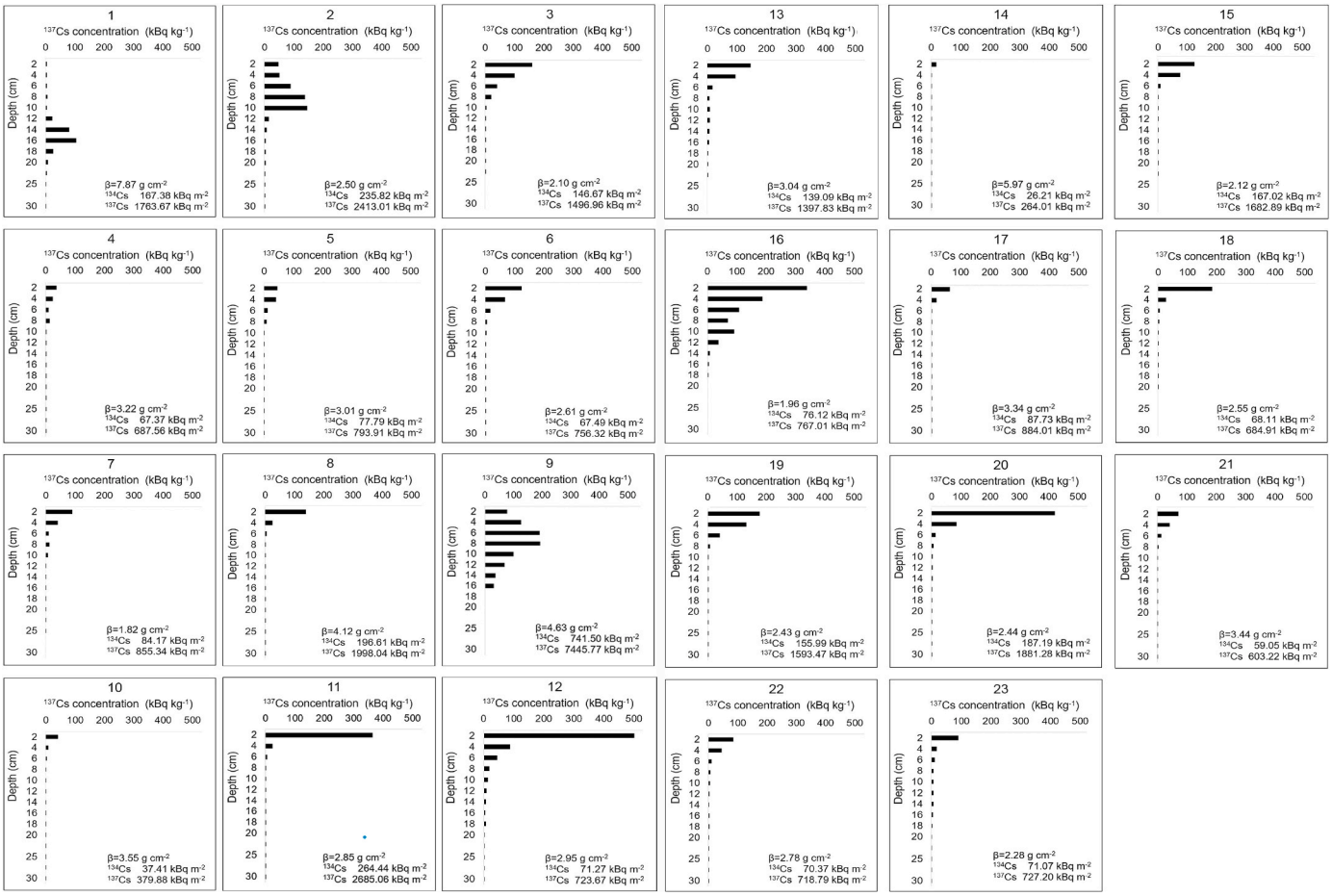

Fig. 10. ^{137}Cs concentrations in each 30 cm soil sample by depth and relaxation mass depth (β: g cm^{-2}) (corresponding to the numbers in Fig. 9).

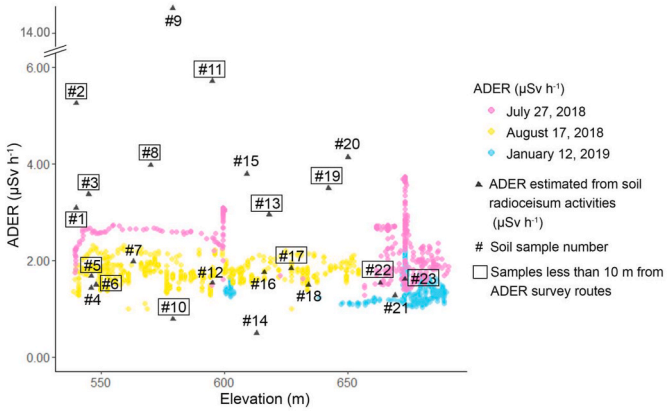

Fig. 11. Scatter plot of actual ADERs (dots) and the estimated ADERs from soil contamination profiles (triangles) with soil sample numbers corresponding to the numbers in Figs. 9 and 10. Soil samples located less than 10 m from air dose survey routes are marked with square boxes.

from soil samples #2 and #11 were also beyond the range of the actual measurements. In soil sample #2, the maximum ^{137}Cs concentration was observed at 8–10 cm depth, while in #11, 92% of total ^{137}Cs activities were in the topmost layer. The variabilities between the ADER estimated from individual soil samples were larger than those between the ADER observed in the field. These excessive over-estimations present a limitation in estimating ADER by using relaxation mass depth (β) from non-exponential radiocesium attenuation curves in locations where surface soil depositions or accelerated downward migration of radiocesium are possible.

Clouvas et al. (1999) found a conversion factor of 1 nGy h^{-1} from ^{137}Cs inventory (1 kBq m^{-2}) to absorbed gamma-ray dose rate using soil samples collected in northern Greece (Antonopoulos-Domis et al., 1997), numerical modeling, and in-situ gamma spectrometry. In this study, the average concentration of ^{137}Cs to 30 cm depth (1,441 kBq m^{-2}) and the average ADER of 1853.33 nSv h^{-1} (1.853 μSv h^{-1}) led to a^{137}Cs inventory to ADER conversion rate of 0.78 nSv h^{-1} for 1 kBq m^{-2}, which is not far from the estimate by Clouvas et al. (1999). These authors cautioned that their factor applied only to forest ecosystems similar to their study forest. This study also cautions readers that our conversion factor is a reference value particular to our study site forest with a limited number of soil samples. Still, it is worth investigating whether the soil depth-averaging method could lead to more accurate ground contamination to ADER estimates than using depth distribution patterns of radionuclides in soils.

3.6. *Implications for future environmental radioactivity measurement and management*

The findings of this study have implications for future ADER measurements and environmental radioactivity management in forested areas.

The first implication is for near-ground survey planning. This study revealed that the median ADER in a forest could vary by more than 1 μSv h^{-1} depending on measurement timing and routes, which are influenced by local topography and meteorological conditions. A one-time survey in part of a forest might not present an accurate picture of ADER distributions in the forest, leading to an inaccurate assessment of radiation exposure risks for humans engaging in forest activities. Therefore multiple near-ground surveys on different survey routes and under different meteorological conditions are necessary to understand the dynamics of radioactivity in forested areas.

The second implication is for ADER survey methods. IAEA TECDOC-1363 (Erdi-Krausz, et al., 2003) suggests that the flight lines of airborne radiation surveys are usually tens of meters to 1 km apart. It is challenging for a high-altitude survey to capture the hotspots that can be captured in a ground survey. For example, the JAEA conducted an airborne survey using a manned helicopter in mid-November 2018, the year in which this study conducted its summer surveys. No precipitation was recorded for 18 days prior to the airborne survey. Mid-November in northeastern Japan is the season of autumn foliage, and deciduous trees have not yet shed all their leaves. A map created from the JAEA data shows that the ADER were in the range of 1.1–2.0 μSv h^{-1} in the study site area (Fig. 12) (JAEA, 2021). In contrast, our surveys recorded ADER above 2.0 μSv h^{-1} on all three survey dates, suggesting that the high-altitude airborne survey did not capture the micro-variations of ADER under the canopy, including hotspots with high levels of radioactivity. Hotspots in forested areas pose higher health risks for residents. Conducting both high-altitude and near-ground ADER surveys in the same forested area as soon as safe access is allowed would enable both rapid wide-area contamination assessments and hotspot risk assessments in a forested topography.

The third implication is the necessity of a 3D topographic approach in ADER modeling. Considering that many nuclear-related facilities are located in remote mountainous areas, if researchers need to understand the consequences of radioactive fallout and radioisotope transport in a forest, incorporating three-dimensional (3D) space features of natural topography into ADER modeling is critical. A limited number of researchers are already embarking on ADER modeling using 3D geometry (Schwarz, et al., 1992; Atarashi-Andoh, et al., 2015; Malins et al., 2015a).

The ground-to-air conversion model used in this study is a well-established methodology. However, the conversion factors are modeled based on a planar ground surface and the assumption that the largest ground contamination is found in the top layers of soils. Malins et al. (2015a) concluded that uneven topographies could lead to a 50% change in the ADER at the height of 300 m compared to a situation where the ground was uniformly flat. Based on numerical models, Schwarz et al. (1992) indicated that ADER measurements in a location surrounded by an ascending slope resulted in higher ADER compared to measurements on a flat and open surface because the radioactive source (the ground) was closer to the detector in the former case. The contrary was true for slopes that descend away from the detector. Even if researchers increase the number of soil samples and estimate ADER from the samples in an area, the estimated environmental radioactivity might not reflect reality if the surrounding angled topography is not considered. It is possible that decontaminating surface soils in flat areas surrounded by slopes will not lead to the intended ADER reduction. In undulating topography where water pooling, sediment accumulation, and surface blocking by snow occur, ground-to-air relation models require additional parameters than vertical migration of radionuclides.

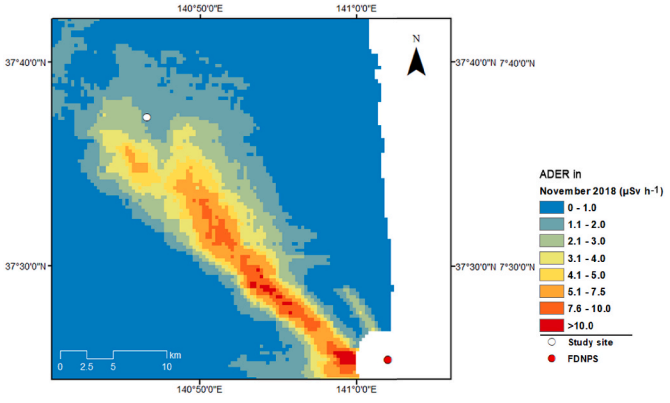

Fig. 12. ADER estimated by airborne survey conducted in November 2018. The map was created using ESRI ArcMap 10.8.1. Data source: JAEA (2021).

4. Conclusions

In this study, we examined the relationships among gamma-ray ADER, topography, and radiocesium contamination levels in soils in a forest in Fukushima prefecture approximately 7.5 years after the FDNPP accident. The hand-held and backpack-type scintillators used in this study enabled near-ground measurement across the undulating surface of the forest. The ADER exceeded the maximum permissible level (0.23 μSv h^{-1}) set by the Japanese government and ranged from 1 μSv h^{-1} to 3.73 μSv h^{-1}. The topographic influences on the ADER were assessed on three dates at the same study site using MARS with five topographic parameters. The study demonstrated the heterogeneous distribution and changeability of the ADER under the canopy. The MARS results suggest that topographic influences could explain at least half of the variability in ADER distribution. Although the survey paths did not completely overlap, the changeability in absolute ADER by date was clearly demonstrated. We concluded that ground wetness contributed to a suppression of the ADER and ADER variability, whereas tree type did not make a significant difference to the rates. Radiocesium contamination levels in soils only partially coincided with the distribution patterns of the actual ADER. About half of the ADER estimated from the soil samples were in the range of actual ADER but lacked a clear correlation with elevation or actual ADER. These results demonstrate that a one-time ADER survey and the existing ground-to-air conversion method may be insufficient for understanding environmental radioactivity pathways and their interactions in a forest. In the quest to decode environmental radioactivity, near-ground ADER measurements can complement high-altitude surveys, helping researchers to better understand the effects of topography on these measurements and, thus, facilitating the development of more accurate environmental radioactivity pathway models.

Author contributions

MY: conceptualization, field data collection, data analysis, writing and editing of original manuscript, and visualization; TN: field data collection and manuscript review; MP: variographical analysis and manuscript review; KO: ground-to-air conversion supervision and manuscript editing; XY: technical review and manuscript editing; JA: methodology supervision and manuscript review; MK: environmental radiology review and manuscript review.

Funding

This work was supported by the NSF Doctoral Dissertation Research Improvement Award - Geography and Spatial Sciences Program (DDRI-GSS) (award number: 1819727) and the College of Arts and Sciences Dissertation Fellowship of the University at Buffalo.

Declaration of competing interest

The authors declare that they have no known competing financial interests or personal relationships that could have appeared to influence the work reported in this paper.

Data availability

Data will be made available on request.

Acknowledgments

Field measurements were accomplished with the support of the Laboratory of Soil Physics and Soil Hydrology at the Graduate School of Agricultural and Life Sciences at the University of Tokyo, Japan. Radioactivity measurement of soil samples was possible with the generous support of the Isotope Facility for Agricultural Education and Research at the Graduate School of the University of Tokyo, Japan. Dr. Naoto Nihei, from Fukushima University, provided the KURAMA II. Mr. Kinichi Okubo, a farmer in Iitate Village, kindly allowed the use of his land for sample and data collection. Geovariances provided the Isatis.neo™ geostatistical software for the variographical analysis.

Appendix A. Supplementary data

Supplementary data to this article can be found online at https://doi.org/10.1016/j.radmeas.2023.106978.

References

Andoh, M., Yamamoto, H., Kanno, T., Saito, K., 2019. Measurement of ambient dose equivalent rates by walk survey around Fukushima Dai-ichi Nuclear Power Plant using KURAMA-II until 2016. J. Environ. Radioact. 210, 105812 https://doi.org/10.1016/j.jenvrad.2018.09.010.

Antonopoulos-Domis, M., Clouvas, A., Xanthos, S., Alifrangis, D.A., 1997. Radiocesium contamination in a submediterranean semi-natural ecosystem following the Chernobyl accident: measurements and models. Health Phys. 72, 243–255. https://doi.org/10.1097/00004032-199702000-00007.

Atarashi-Andoh, M., Koarashi, J., Takeuchi, E., Tsuduki, K., Nishimura, S., Matsunaga, T., 2015. Catchment-scale distribution of radiocesium air dose rate in a mountainous deciduous forest and its relation to topography. J. Environ. Radioact. 147, 1–7. https://doi.org/10.1016/j.jenvrad.2015.05.004.

Azmi, D.I., Karim, H.A., Amin, M.Z.M., 2012. Comparing the walking behaviour between urban and rural residents. Procedia Soc. Behav. Sci. 68, 406–416. https://doi.org/10.1016/j.sbspro.2012.12.237.

Bailly du Bois, P., Laguionie, P., Boust, D., Korsakissok, I., Didier, D., 2012. Estimation of marine source-term following Fukushima Dai-ichi accident. J. Environ. Radioact. 114, 2–9. https://doi.org/10.1016/j.jenvrad.2011.11.015.

Baldoncini, M., Albéri, M., Bottardi, C., Chiarelli, E., Raptis, K.G.C., Strati, V., Mantovani, F., 2018. Investigating the potentialities of Monte Carlo simulation for assessing soil water content via proximal gamma-ray spectroscopy. J. Environ. Radioact. 192, 105–116. https://doi.org/10.1016/j.jenvrad.2018.06.001.

Baldoncini, M., Albéri, M., Bottardi, C., Chiarelli, E., Raptis, K.G.C., Strati, V., Mantovani, F., 2019. Biomass water content effect on soil moisture assessment via proximal gamma-ray spectroscopy. Geoderma 335, 69–77. https://doi.org/10.1016/j.geoderma.2018.08.012.

Basuki, T., Bekelesi, W.C., Tsujimoto, M., Nakashima, S., 2020. Air dose rate to ^{137}Cs activity per unit area ratio for different land use 7 years after the nuclear accident – case of the slope catchment, Ogi reservoir, Fukushima. Radiat. Meas. 137, 106424 https://doi.org/10.1016/j.radmeas.2020.106424.

Beck, H.E., Zimmermann, N.E., McVicar, T.R., Vergopolan, N., Berg, A., Wood, E.F., 2018. Present and future Köppen-Geiger climate classification maps at 1-km resolution. Sci. Data 5 (1), 1–12. https://doi.org/10.1038/sdata.2018.214.

Bivand, R.S., Pebesma, E.J., Gómez-Rubio, V., Pebesma, E.J., 2008. Applied Spatial Data Analysis with R, vol. 747248717. Springer, New York.

Carroll, T.R., 1981. Airborne soil moisture measurement using natural terrestrial gamma radiation. Soil Sci. 132, 358–366. https://doi.org/10.1097/00010694-198111000-00006.

Chibowski, S., Zygmunt, J., Klimowicz, Z., 1999. Investigation of adsorption and vertical migration of ^{137}Cs in three kinds of soil at Lublin vicinity. J. Radioanal. Nucl. Chem. 242, 287–295. https://doi.org/10.1007/bf02345555.

Chino, M., Terada, H., Nagai, H., Katata, G., Mikami, S., Torii, T., Saito, K., Nishizawa, Y., 2011. Preliminary estimation of release amounts of ^{131}I and ^{137}Cs accidently discharged from the Fukushima Daiichi nuclear power plant into the atmosphere. J. Nucl. Sci. Technol. 48, 1129–1134. https://doi.org/10.1080/18811248.2011.9711799.

Clouvas, A., Xanthos, S., Antonopoulos-Domis, M., Alifragis, D.A., 1999. Contribution of the 137Cs to the total absorbed gamma dose rate in air in a Greek forest ecosystem: measurements and Monte Carlo computations. Health Phys. 76, 36–43. https://doi.org/10.1097/00004032-199901000-00006.

Conrad, O., Bechtel, B., Bock, M., Dietrich, H., Fischer, E., Gerlitz, L., Wehberg, J., Wichmann, V., Bohner, J., 2015. System for Automated Geoscientific Analyses (SAGA) V. 2.1.4. Geosci. Model Dev. 8. 1991–2007. https://doi.org/10.5194/gmd-8-1991-2015.

Cressie, N., 1986. Kriging nonstationary data. J. Am. Stat. Assoc. 81, 625–634. https://doi.org/10.1080/01621459.1986.10478315.

Cruz-Suarez, R., Gustafsson, M., Mrabit, K., 2001. IAEA occupational radiation protection programme. Radiat. Protect. Dosim. 96, 17–20. https://doi.org/10.1093/oxfordjournals.rpd.a006575.

Daniels, R.D., Schubauer-Berigan, M.K., 2011. A meta-analysis of leukaemia risk from protracted exposure to low-dose gamma radiation. Occup. Environ. Med. 68, 457–464. https://doi.org/10.1136/oem.2009.054684.

Erdi-Krausz, G., Matolin, M., Minty, B., Nicolet, J., Reford, W., Schetselaar, E., 2003. Guidelines for Radioelement Mapping Using Gamma Ray Spectrometry Data. Also as open access e-book. International Atomic Energy Agency.

Friedman, J.H., 1991. Multivariate adaptive regression splines. Ann. Stat. 1–67 https://doi.org/10.1214/aos/1176347963.

Fujiwara, H., Kuramochi, H., Nomura, K., Maeseto, T., Osako, M., 2017. Behavior of radioactive cesium during incineration of radioactively contaminated wastes from

decontamination activities in Fukushima. J. Environ. Radioact. 178–179, 290–296. https://doi.org/10.1016/j.jenvrad.2017.08.014.
Furukawa, M., Shingaki, R., 2012. Terrestrial gamma radiation dose rate in Japan estimated before the 2011 Great East Japan Earthquake. Radiat. Emerg. Med. 1, 11–16.
Geovariances, 2021. In: Isatis.neo. Available from. https://www.geovariances.com/en/software/isatis-neo-geostatistics-software/.
Gessler, P.E., Moore, I.D., McKenzie, N.J., Ryan, P.J., 1995. Soil-landscape modelling and spatial prediction of soil attributes. Int. J. Geogr. Inf. Syst. 9, 421–432. https://doi.org/10.1080/02693799508902047.
Goovaerts, P., 2000. Geostatistical approaches for incorporating elevation into the spatial interpolation of rainfall. J. Hydrol. 228, 113–129. https://doi.org/10.1016/s0022-1694(00)00144-x.
Hanna, S.R., Briggs, G.A., Hosker, R.P., 1982. Handbook on Atmospheric Diffusion, vol. 11223. Technical information center of the US Department of Energy DOE. TIC. https://doi.org/10.2172/5591108.
Hashimoto, S., Ugawa, S., Nanko, K., Shichi, K., 2012. The total amounts of radioactively contaminated materials in forests in Fukushima, Japan. Sci. Rep. 2, 416. https://doi.org/10.1038/srep00416.
Hashimoto, S., Komatsu, M., Miura, S., 2022. The future of forests in Fukushima: how should we face radioactive contamination of forests. In: Forest Radioecology in Fukushima. Springer, Singapore. https://doi.org/10.1007/978-981-16-9404-2_7.
Hastie, T.J., Tibshirani, R., 1986. Generalized additive models. Stat. Sci. 1, 297–318.
He, Q., Walling, D.E., 1996. Interpreting particle size effects in the adsorption of 137Cs and unsupported 210Pb by mineral soils and sediments. J. Environ. Radioact. 30, 117–137. https://doi.org/10.1016/0265-931x(96)89275-7.
Heimsath, A.M., Dietrich, W., Nishiizumi, K., Finkel, R., 1997. The soil production function and landscape equilibrium. Nature 388, 358. https://doi.org/10.1038/41056.
Heimsath, A.M., Dietrich, W.E., Nishiizumi, K., Finkel, R.C., 1999. Cosmogenic nuclides, topography, and the spatial variation of soil depth. Geomorphology 27, 151–172. https://doi.org/10.1016/s0169-555x(98)00095-6.
IAEA, 2015. The Fukushima Daiichi accident. In: Technical, 4/5. Radiological Consequences, Vienna, Austria.
ICRU, 1994. Gamma-ray spectrometry in the environment. In: International Commission on Radiation Units and Measurements (ICRU) Report, vol. 53. Bethesda, Maryland.
Ii, I., Nihei, N., Hirose, A., Kobayashi, N., Kanno, M., Mizoguchi, M., 2021. Annual reduction of transfer factor of radiocesium from Soil to Rice Cultivated in a KCl fertilized paddy field from 2015 to 2019. Radioisotopes 70, 63–72. https://doi.org/10.3769/radioisotopes.70.63.
Imamura, N., Matsuura, T., Akama, A., Ikeda, S., Kobayashi, M., Miura, S., Shinomiya, Y., Kaneko, S., 2020. Temporal changes in the spatial patterns of air dose rate from 2012 to 2016 at forest floors in Fukushima, Japan. J. Environ. Radioact. 222, 106377 https://doi.org/10.1016/j.jenvrad.2020.106377.
Imanaka, T., Endo, S., Sugai, M., Ozawa, S., Shizuma, K., Yamamoto, M., 2012. Early radiation survey of Iitate village, which was heavily contaminated by the Fukushima Daiichi accident, conducted on 28 and 29 March 2011. Health Phys. 102, 680–686. https://doi.org/10.1097/HP.0b013e31824cfe18.
Isaaks, E.H., Srivastava, R.M., 1989. An Introduction to Applied Geostatistics. Oxford University Press.
Ishizaki, A., Sanada, Y., Mori, A., Imura, M., Ishida, M., Munakata, M., 2016. Investigation of snow cover effects and attenuation correction of gamma ray in aerial radiation monitoring. Rem. Sens. 8, 892. https://doi.org/10.3390/rs8110892.
Istanbulluoglu, E., Yetemen, O., Vivoni, E.R., Gutiérrez-Jurado, H.A., Bras, R.L., 2008. Eco-geomorphic implications of hillslope aspect: inferences from analysis of landscape morphology in central New Mexico. Geophys. Res. Lett. 35, L14403 https://doi.org/10.1029/2008gl034477.
IUSS Working Group, 2015. World Reference Base for Soil Resources 2014, Update 2015. International Soil Classification System for Naming Soils and Creating Legends for Soil Maps. World Soil Resources Reports, Rome. FAO.
Jacob, P., Debertin, K., Miller, K., Roed, J., Saito, K., Sanderson, D., 1994. Ground-level gamma-ray spectrometry. J. ICRU. os-27 15–27. https://doi.org/10.1093/jicru_os27.2.15.
JAEA, 2021. Database for Radioactive Substance Monitoring Data. https://emdb.jaea.go.jp/emdb. (Accessed 11 November 2022).
Jagercikova, M., Evrard, O., Balesdent, J., Lefèvre, I., Cornu, S., 2014. Modeling the migration of fallout radionuclides to quantify the contemporary transfer of fine particles in Luvisol profiles under different land uses and farming practices. Soil Tillage Res. 140, 82–97. https://doi.org/10.1016/j.still.2014.02.013.
Japan Meteorological Agency, 2019. In: Data and References. http://www.jma.go.jp/jma/menu/menureport.html. (Accessed 2 September 2019).
Ji, Y.Y., Kim, C.J., Chung, K.H., Choi, H.Y., Lee, W., Kang, M.J., Park, S.T., 2016. In situ gamma-ray spectrometry in the environment using dose rate spectroscopy. Radiat. Phys. Chem. 119 https://doi.org/10.1016/j.radphyschem.2015.10.001, 90–02.
Kato, H., Onda, Y., Teramage, M., 2012. Depth distribution of ^{137} Cs, ^{134} Cs, and ^{131} I in soil profile after Fukushima Dai-ichi nuclear power plant accident. J. Environ. Radioact. 111, 59–64. https://doi.org/10.1016/j.jenvrad.2011.10.003.
Kato, H., Onda, Y., Hisadome, K., Loffredo, N., Kawamori, A., 2017. Temporal changes in radiocesium deposition in various forest stands following the Fukushima Dai-ichi Nuclear Power Plant accident. J. Environ. Radioact. 166, 449–457. https://doi.org/10.1016/j.jenvrad.2015.04.016.
Kato, H., Onda, Y., Wakahara, T., Kawamori, A., 2018a. Spatial pattern of atmospherically deposited radiocesium on the forest floor in the early phase of the Fukushima Daiichi Nuclear Power Plant accident. Sci. Total Environ. 615, 187–196. https://doi.org/10.1016/j.scitotenv.2017.09.212.
Kato, H., Onda, Y., Yamaguchi, T., 2018b. Temporal changes of the ambient dose rate in the forest environments of Fukushima Prefecture following the Fukushima reactor accident. J. Environ. Radioact. 193, 20–26. https://doi.org/10.1016/j.jenvrad.2018.08.009.
Kato, H., Onda, Y., Gao, X., Sanada, Y., Saito, K., 2019. Reconstruction of a Fukushima accident-derived radiocesium fallout map for environmental transfer studies. J. Environ. Radioact. 210, 105996 https://doi.org/10.1016/j.jenvrad.2019.105996.
Koarashi, J., Atarashi-Andoh, M., Matsunaga, T., Sato, T., Nagao, S., Nagai, H., 2012. Factors affecting vertical distribution of Fukushima accident-derived radiocesium in soil under different land-use conditions. Sci. Total Environ. 431, 392–401. https://doi.org/10.1016/j.scitotenv.2012.05.041.
Koarashi, J., Atarashi-Andoh, M., Matsunaga, T., Sanada, Y., 2016. Forest type effects on the retention of radiocesium in organic layers of forest ecosystems affected by the Fukushima nuclear accident. Sci. Rep. 6, 1–11. https://doi.org/10.1038/srep38591.
Komissarov, M.A., Ogura, S., 2017. Distribution and migration of radiocesium in sloping landscapes three years after the Fukushima-1 nuclear accident. Eurasian Soil Sci. 50, 861–871. https://doi.org/10.1134/s1064229317070043.
Komissarov, M.A., Ogura, S., 2020. Soil erosion and radiocesium migration during the snowmelt period in grasslands and forested areas of Miyagi prefecture, Japan. Environ. Monit. Assess. 192, 1–15. https://doi.org/10.1007/s10661-020-08542-5.
Konoplev, A.V., Golosov, V.N., Yoschenko, V.I., Nanba, K., Onda, Y., Takase, T., Wakiyama, Y., 2016. Vertical distribution of radiocesium in soils of the area affected by the Fukushima Dai-ichi nuclear power plant accident. Eurasian Soil Sci. 49, 570–580. https://doi.org/10.1134/S1064229316050082.
Korobova, E., Ermakov, A., Linnik, V., 1998. ^{137}Cs and ^{90}Sr mobility in soils and transfer in soil–plant systems in the Novozybkov district affected by the Chernobyl accident. Appl. Geochem. 13, 803–814. https://doi.org/10.1016/s0883-2927(98)00021-3.
Korobova, E., Linnik, V., Chizhikova, N., 2007. The history of the Chernobyl ^{137}Cs contamination of the flood plain soils and its relation to physical and chemical properties of the soil horizons (a case study). J. Geochem. Expl. 96, 236–255. https://doi.org/10.1016/j.gexplo.2007.04.014.
Kurihara, M., Onda, Y., Suzuki, H., Iwasaki, Y., Yasutaka, T., 2018. Spatial and temporal variation in vertical migration of dissolved ^{137}Cs passed through the litter layer in Fukushima forests. J. Environ. Radioact. 192, 1–9. https://doi.org/10.1016/j.jenvrad.2018.05.012.
Leathwick, J.R., Elith, J., Hastie, T., 2006. Comparative performance of generalized additive models and multivariate adaptive regression splines for statistical modelling of species distributions. Ecol. Model. 199, 188–196. https://doi.org/10.1016/j.ecolmodel.2006.05.022.
Maekawa, A., Momoshima, N., Sugihara, S., Ohzawa, R., Nakama, A., 2015. Analysis of 134 Cs and 137 Cs distribution in soil of Fukushima prefecture and their specific adsorption on clay minerals. J. Radioanal. Nucl. Chem. 303, 1485–1489. https://doi.org/10.1007/s10967-014-3575-2.
Malins, A., Okumura, M., Machida, M., Saito, K., 2015a. Topographic effects on ambient dose equivalent rates from radiocesium fallout. In: Proceedings of Joint International Conference on Mathematics and Computation, Supercomputing in Nuclear Applications and the Monte Carlo Method. M&C + SNA + MC 2015.
Malins, A., Okumura, M., Machida, M., Takemiya, H., Saito, K., 2015b. Fields of View for Environmental Radioactivity. https://doi.org/10.48550/arXiv.1509.09125. Preprint ArXiv:1509.09125.
Martin, Y., 2000. Modelling hillslope evolution: linear and nonlinear transport relations. Geomorphology 34, 1–21. https://doi.org/10.1016/s0169-555x(99)00127-0.
Melese Endalew, A., Hertog, M., Verboven, P., Baetens, K., Delele, M.A., Ramon, H., Nicolai, B., 2006. Modelling airflow through 3D canopy structure of orchards. Aspect Appl. Biol. 77, 465–472. https://doi.org/10.1615/ichmt.2009.turbulheatmasstransf.1240.
Melese Endalew, A., Hertog, M., Delele, M.A., Baetens, K., Persoons, T., Baelmans, M., Ramon, H., Nicolaï, B.M., Verboven, P., 2009. CFD modelling and wind tunnel validation of airflow through plant canopies using 3D canopy architecture. Int. J. Heat Fluid Flow 30, 356–368. https://doi.org/10.1016/j.ijheatfluidflow.2008.12.007.
Mikailova, R., Onda, Y., Fesenko, S., Kato, H., 2021. Absorbed Dose Rate Assessment for the Japanese Cedar Stand Affected after the Fukushima NPP Accident. https://doi.org/10.5194/egusphere-egu21-10529. EGU General Assembly Conference Abstracts. EGU21-10529.
Milborrow, S., 2020. Earth: Multivariate Adaptive Regression Splines.
Ministry of Agriculture, Forestry and Fisheries, Japan, 2017. In: Natural and Artificial Forest Areas by Prefectures. https://www.rinya.maff.go.jp/j/keikaku/genkyou/h29/1.html. (Accessed 1 October 2021).
Momm, H.G., Bingner, R.L., Wells, R.R., Wilcox, D., 2012. AGNPS GIS-based tool for watershed-scale identification and mapping of cropland potential ephemeral gullies. Appl. Eng. Agric. 28, 17–29. https://doi.org/10.13031/2013.41282.
Moore, I.D., Gessler, P.E., Nielsen, G.A., Peterson, G.A., 1993. Soil attribute prediction using terrain analysis. Soil Sci. Soc. Am. J. 57, 443–452. https://doi.org/10.2136/sssaj1993.03615995005700020058x.
Nagaoka, T., Sakamoto, R., Saito, K., Tsutsumi, M., Moriuchi, S., 1988. Diminution of terrestrial gamma ray exposure rate due to snow cover. Jpn. J. Health Phys. 23, 309–315. https://doi.org/10.5453/jhps.23.309 (in Japanese).
Nakanishi, T., Matsunaga, T., Koarashi, J., Atarashi-Andoh, M., 2014. ^{137}Cs vertical migration in a deciduous forest soil following the Fukushima Dai-ichi Nuclear Power Plant accident. J. Environ. Radioact. 128, 9–14. https://doi.org/10.1016/j.jenvrad.2013.10.019.
Nakanishi, M., Onda, Y., Kato, H., Takahashi, J., Ida, H., 2022. Changes in air dose rates due to changes in soil moisture content in forests in Fukushima Prefecture. In: The Japanese Forest Society Congress 133rd Annual JFS Meeting. The Japanese Forestry Society, p. 47. https://doi.org/10.11519/jfsc.133.0_47.

Nakano, M., Povinec, P.P., 2012. Long-term simulations of the ^{137}Cs dispersion from the Fukushima accident in the world ocean. J. Environ. Radioact. 111, 109–115. https://doi.org/10.1016/j.jenvrad.2011.12.001.

Ochi, K., Funaki, H., Yoshimura, K., Iimoto, T., Matsuda, N., Sanada, Y., 2022. Validation study of ambient dose equivalent conversion coefficients for radiocaesium distributed in the ground: lessons from the Fukushima Daiichi Nuclear Power Station accident. Radiat. Environ. Biophys. 61, 147–159. https://doi.org/10.1007/s00411-022-00969-3.

Omori, Y., Wakamatsu, H., Sorimachi, A., Ishikawa, T., 2016. Radiation survey on Fukushima Medical University premises about four years after the Fukushima nuclear disaster. Fukushima J. Med. Sci. 62, 1–17. https://doi.org/10.5387/fms.2015-16.

Osawa, K., Nonaka, Y., Nishimura, T., Tanoi, K., Matsui, H., Mizogichi, M., Tatsuno, T., 2018. Quantification of dissolved and particulate radiocesium fluxes in two rivers draining the main radioactive pollution plume in Fukushima, Japan (2013–2016). Anthropocene 22, 40–50. https://doi.org/10.1016/j.ancene.2018.04.003.

Quine, T.A., Govers, G., Walling, D.E., Zhang, X., Desmet, P.J.J., Zhang, Y., Vandaele, K., 1997. Erosion processes and landform evolution on agricultural land – new perspectives from caesium-137 measurements and topographic-based erosion modelling. Earth Surf. Process. Landforms 22, 799–816. https://doi.org/10.1002/(SICI)1096-9837(199709)22:9<799::AID-ESP765>3.0.CO;2-R.

R Core Team, 2018. R: A Language and Environment for Statistical Computing. R Foundation for Statistical Computing, Vienna, Austria.

Ritchie, J.C., McHenry, J.R., 1990. Application of radioactive fallout cesium-137 for measuring soil erosion and sediment accumulation rates and patterns: a review. J. Environ. Qual. 19, 215–233. https://doi.org/10.2134/jeq1990.00472425001900020006x.

Roering, J.J., Kirchner, J.W., Dietrich, W.E., 1999. Evidence for nonlinear, diffusive sediment transport on hillslopes and implications for landscape morphology. Water Resour. Res. 35, 853–870. https://doi.org/10.1029/1998wr900090.

Roering, J., Kirchner, J., Dietrich, W., 2001. Hillslope evolution by nonlinear, slope-dependent transport: steady state morphology and equilibrium adjustment timescales. J. Geophys. Res. Solid Earth 106, 16499–16513. https://doi.org/10.1029/2001jb000323.

Saito, K., Petoussi-Henss, N., 2014. Ambient dose equivalent conversion coefficients for radionuclides exponentially distributed in the ground. J. Nucl. Sci. Technol. 51, 1274–1287. https://doi.org/10.1080/00223131.2014.919885.

Sanada, Y., Katata, G., Kaneyasu, N., Nakanishi, C., Urabe, Y., Nishizawa, Y., 2018. Altitudinal characteristics of atmospheric deposition of aerosols in mountainous regions: lessons from the Fukushima Daiichi Nuclear Power Station accident. Sci. Total Environ. 618, 881–890. https://doi.org/10.1016/j.scitotenv.2017.08.246.

Sanada, Y., Urabe, Y., Sasaki, M., Ochi, K., Torii, T., 2019. Evaluation of ecological half-life of dose rate based on airborne radiation monitoring following the Fukushima Dai-ichi nuclear power plant accident. J. Environ. Radioact. 210, 105816 https://doi.org/10.1016/j.jenvrad.2018.07.016.

Sanada, Y., Yoshimura, K., Urabe, Y., Iwai, T., Katengeza, E.W., 2020. Distribution map of natural gamma-ray dose rates for studies of the additional exposure dose after the Fukushima Dai-ichi Nuclear Power Station accident. J. Environ. Radioact. 223, 106397 https://doi.org/10.1016/j.jenvrad.2020.106397.

Sasaki, M., Ishizaki, A., Sanada, Y., 2019. Development of analysis method for airborne radiation monitoring using the inverse problem solutions. Prog. Nucl. Sci. Technol. 6, 63–67. https://doi.org/10.15669/pnst.6.63.

Sato, T., Andoh, M., Sato, M., Saito, K., 2019. External dose evaluation based on detailed air dose rate measurements in living environments. J. Environ. Radioact. 210, 105973 https://doi.org/10.1016/j.jenvrad.2019.05.005.

Schimmack, W., Bunzl, K., Dietl, F., Klotz, D., 1994. Infiltration of radionuclides with low mobility (^{137}Cs and ^{60}Co) into a forest soil. Effect of the irrigation intensity. J. Environ. Radioact. 24, 53–63. https://doi.org/10.1016/0265-931x(94)90024-8.

Schimmack, W., Steindl, H., Bunzl, K., 1998. Variability of water content and of depth profiles of global fallout ^{137}Cs in grassland soils and the resulting external gamma dose rates. Radiat. Environ. Biophys. 37, 27–33. https://doi.org/10.1007/s004110050088.

Schwarz, G.F., Klingelé, E., Rybach, L., 1992. How to handle rugged topography in airborne gamma-ray spectrometry surveys. First Break 10 (1), 11–17. https://doi.org/10.3997/1365-2397.1992001.

Somboon, S., Kavasi, N., Sahoo, S.K., Inoue, K., Arae, H., Tsuruoka, H., Shimizu, H., Fukushi, M., 2018. Radiocesium and ^{40}K distribution of river sediments and floodplain deposits in the Fukushima exclusion zone. J. Environ. Radioact. 195, 40–53. https://doi.org/10.1016/j.jenvrad.2018.09.003.

Stone, J.J., Hawkins, R.H., Shirley, E.D., 1994. Approximate form of Green-Ampt infiltration equation. J. Irrigat. Drain. Eng. 120, 128–137. https://doi.org/10.1061/(ASCE)0733-9437(1994)120:1(128).

Sun, D., Wainwright, H., Suresh, I., Seki, A., Takemiya, H., Saito, K., 2022. Spatial and temporal prediction of radiation dose rates near Fukushima Daiichi Nuclear Power Plant. J. Environ. Radioact. 251, 106946 https://doi.org/10.1016/j.jenvrad.2022.106946.

Tanaka, M., Matsubara, S., 2012. The characteristics and handling of a survey meter. Isotope news 694, 32–38.

Tanigaki, M., Okumura, R., Takamiya, K., Sato, N., Yoshino, H., Yoshinaga, H., Kobayashi, Y., Uehara, A., Yamana, H., 2015. Development of KURAMA-II and its operation in Fukushima. Nucl. Instrum. Methods Phys. Res. 781, 57–64. https://doi.org/10.1016/j.nima.2015.01.086.

Tarboton, D.G., 2005. TauDEM (Terrain Analysis Using Digital Elevation Models). Utah State University, Logan, Utah.

Teramage, M.T., Onda, Y., Patin, J., Kato, H., Gomi, T., Nam, S., 2014. Vertical distribution of radiocesium in coniferous forest soil after the Fukushima nuclear power plant accident. J. Environ. Radioact. 137, 37–45. https://doi.org/10.1016/j.jenvrad.2014.06.017.

Tesfa, T.K., Tarboton, D.G., Chandler, D.G., McNamara, J.P., 2009. Modeling soil depth from topographic and land cover attributes. Water Resour. Res. 45, 1–16. https://doi.org/10.1029/2008wr007474.

Tobler, W.R., 1970. A computer movie simulating urban growth in the Detroit region. Econ. Geogr. 46, 234–240. https://doi.org/10.2307/143141.

Tsuda, T., Tokinobu, A., Yamamoto, E., Suzukib, E., 2015. Thyroid cancer detection by ultrasound among residents ages 18 Years and younger in Fukushima, Japan: 2011 to 2014. Epidemiology 27, 316–322. https://doi.org/10.1097/ede.0000000000000385.

Valentin, J., 2005. Low-dose extrapolation of radiation-related cancer risk. Ann. ICRP 35, 1–140. https://doi.org/10.1016/j.icrp.2005.11.002.

Walling, D.E., He, Q., Quine, T., 1996. Use of fallout radionuclide measurements in sediment budget investigations/La mesure des retombées de radionucléides: un outil pour l'évaluation des bilans sédimentaires. Geomorphologie 2, 17–27. https://doi.org/10.3406/morfo.1996.882.

Walling, D.E., He, Q., 1999. Improved models for estimating soil erosion rates from cesium-137 measurements. J. Environ. Qual. 28, 611–622. https://doi.org/10.2134/jeq1999.00472425002800020027x.

Yamada, T., 1982. A numerical model study of turbulent airflow in and above a forest canopy. J. Meteorol. Soc. Jpn. 60, 439–454. https://doi.org/10.2151/jmsj1965.60.1_439.

Yasumiishi, M., Nishimura, T., Aldstadt, J., Bennett, S.J., Bittner, T., 2021. Assessing the effect of topography on Cs-137 concentrations within forested soils due to the Fukushima Daiichi Nuclear Power Plant accident, Japan. Earth Surf. Dyn. 9, 861–893. https://doi.org/10.5194/esurf-9-861-2021.

Yasutaka, T., Naito, W., 2016. Assessing cost and effectiveness of radiation decontamination in Fukushima Prefecture, Japan. J. Environ. Radioact. 151, 512–520. https://doi.org/10.1016/j.jenvrad.2015.05.012.

Yoschenko, V., Nanba, K., Wada, T., Johnson, T.E., Zhang, J., Workman, D., Nagata, H., 2022. Late phase radiocesium dynamics in Fukushima forests post deposition. J. Environ. Radioact. 251–252, 106947 https://doi.org/10.1016/j.jenvrad.2022.106947.

Yoshimura, K., 2022. Air dose rates and cesium-137 in urban areas – deposition, migration, and time dependencies after nuclear power plant accidents. J. Nucl. Sci. Technol. 59, 25–33. https://doi.org/10.1080/00223131.2021.1973608.

Yoshioka, K., 1994. Study of time variation of terrestrial gamma radiation due to depth distribution of soil moisture content. Radioisotopes 43 (4), 183–189. https://doi.org/10.3769/radioisotopes.43.183.